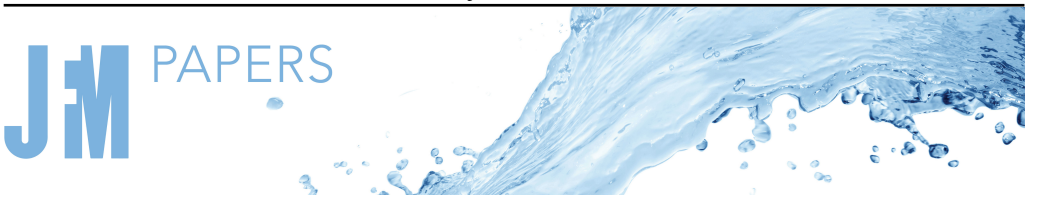
J. Fluid Mech. (2026), *vol.* 1032, A34, doi:10.1017/jfm.2026.11340



Maxwell–Cattaneo double-diffusive convection: the general case

D.W. Hughes[1], **M.R.E. Proctor**[2] **and I.A. Eltayeb**[3]

[1]School of Mathematics, University of Leeds, Leeds LS2 9JT, UK

[2]DAMTP, Centre for Mathematical Sciences, Wilberforce Road, Cambridge CB3 0WA, UK

[3]Faculty of Mathematical Sciences and Informatics, University of Khartoum, POB 321, Khartoum, Sudan

Corresponding author: D.W. Hughes, d.w.hughes@leeds.ac.uk

(Received 28 August 2025; revised 10 February 2026; accepted 16 February 2026)

Double-diffusive convection, in which the density of a fluid is dependent on two fields that diffuse at different rates (such as temperature and salinity), has been widely studied in areas as diverse as the oceans and stellar atmospheres. Under the assumption of classical Fickian diffusion for both heat and salt, the evolution of temperature and salinity is governed by parabolic advection–diffusion equations. In reality, there are small additional terms in these equations that render them hyperbolic (the Maxwell–Cattaneo (M–C) effect). Although these corrections are nominally small, they represent a singular perturbation, and hence can lead to significant effects when the underlying differences of salinity and temperature are large. In an earlier paper (Hughes, Proctor & Eltayeb, *J. Fluid Mech.*, vol. 927, 2021, p. A13), we investigated the linear stability of a double-diffusive fluid layer subject to the M–C effect in either the temperature or the salinity equation (but not both). Here we consider the general, and much more complicated, case in which the M–C effect influences both temperature and salinity. We find that, as in the earlier paper, oscillatory instability is indeed facilitated (and in fact made possible when the salinity gradient is destabilising, where the classical problem has no oscillatory instability) when the salinity gradients are sufficiently large. The scalings that emerge from the earlier paper, however, are not necessarily representative of those in the general case, thus justifying the present study. In addition, we have found a remarkable singular situation when the ratio of the M–C effects is equal to the ratio between the heat and salinity diffusivities, near which the critical wavenumber is sharply reduced. In addition to determining the stability boundaries we have also investigated the growth rates of unstable modes and shown that these are on a par with those of classical double-diffusive convection.

Key words: double diffusive convection, general fluid mechanics

© The Author(s), 2026. Published by Cambridge University Press. This is an Open Access article, distributed under the terms of the Creative Commons Attribution licence (https://creativecommons.org/licenses/by/4.0/), which permits unrestricted re-use, distribution and reproduction, provided the original article is properly cited.

https://doi.org/10.1017/jfm.2026.11340 Published online by Cambridge University Press

1. Introduction

Double-diffusive convection, driven by density variations that are dependent on two fields that diffuse at different rates, is an important process in many geophysical and astrophysical contexts. The most widely studied such problem, applicable to ocean dynamics, is that of thermohaline convection, in which the rapidly diffusing component is heat and the slowly diffusing component salinity (e.g. Huppert & Turner 1981; Radko 2013). Double-diffusive convection in which the competing elements are the variations in composition and temperature can play a role in the planetary context of crystallisation in magmas (Huppert & Sparks 1984) and in the astrophysical context of mixing in the dynamics of deep stellar interiors (e.g. Kato 1966; Merryfield 1995; Garaud 2018). Interchange instabilities driven by magnetic buoyancy, in which the density depends on variations in magnetic pressure and entropy, and which are believed to be important for the release of magnetic flux from stellar interiors, can also, after a transformation of the governing variables, be understood in terms of the classical double-diffusive problem (see Hughes & Proctor 1988; Hughes & Brummell 2021).

Problems in double-diffusive convection have been extensively investigated over the last half-century, with the common feature that the buoyancy-affecting fields diffuse according to the classic Fickian law (for heat transport, also known as the Fourier law), in which the flux of heat or salt is directly proportional to the temperature or salinity gradient. The temperature T, for example, then obeys the diffusion–advection equation $\mathrm{D}T/\mathrm{D}t = \boldsymbol{\nabla}\cdot((K/\rho c_p)\boldsymbol{\nabla}T)$, where $\mathrm{D}/\mathrm{D}t$ is the usual Lagrangian derivative, K is the thermal conductivity, ρ is the density and c_p is the specific heat at constant pressure. This parabolic equation is necessarily an approximation: it violates relativity, for example, in that information is propagated at infinite speed; nor does it properly account for the detailed nature of heat transport in materials. Maxwell (1867) proposed an improved formulation that replaced the instantaneous nature of the Fickian flux-gradient relation by a modified form in which the flux adjusts in a finite relaxation time τ_T; the usual Fickian law is recovered by setting $\tau_T = 0$. The accuracy of the Fourier law for experiments involving simple classical fluids suggests that τ_T is usually very small, as shown in Carrassi & Morro (1972), where it is suggested that τ_T can be as small as 10^{-9} s for gases. However, for more complex fluids, τ_T can be much larger. For example, Neuhauser (1987), in her investigation of thermal relaxation in superfluid helium-3, found that τ_T has values in the range 30−400 s; Mohammadein (2006), in his study of the thermal relaxation time in two-phase bubbly flow, found that the relaxation time varied between 10^{-3} s and 3 s. The reader is referred to Hughes, Proctor & Eltayeb (2021) (hereinafter referred to as HPE21) for a fuller discussion of the many related earlier papers that include the Maxwell–Cattaneo (M–C) effect for temperature.

Maxwell's formulation (now known as the M–C effect), refined by Christov (2009), leads to unchanged stability criteria for direct (steady) bifurcations from a stationary state with vertical buoyancy gradients, but permits new oscillatory instabilities in certain cases. While the correction term is very small in many instances, it can become important when the density gradients due to heat and salinity are very large. A first attempt at understanding the role of the M–C effect in determining the threshold for double-diffusive instability was made by HPE21. They investigated the effect on the linear stability boundary in the two special cases where the M–C formulation was applied either to the temperature field alone or the salinity field alone. The importance of the new effect is measured (in the case of temperature) by the dimensionless quantity $C_T = \tau_T K/(2\rho c_p d^2) = \tau_T \kappa/2d^2$, where d is a typical length scale and κ is the thermal diffusivity (ρ and K are now assumed constant). Analogous remarks apply to the salinity field, leading to the equivalent

https://doi.org/10.1017/jfm.2026.11340 Published online by Cambridge University Press

coefficient $C_S = \tau_S \kappa_S / 2d^2$, where τ_S is the relaxation time for the salinity and κ_S is the salt diffusivity. Experimental estimates for τ_S remain elusive. We shall be concerned with simple Newtonian fluids, for which C_T and C_S will be very small.

In HPE21 it is shown that, even when C_S or C_T is very small, M–C effects can become significant provided that the salt Rayleigh number Rs, measuring the buoyancy gradient due to salinity, is large, in that $RsC^n = O(1)$, where $n \geqslant 1$ and C denotes either C_T or C_S. In HPE21 the two limiting cases, in which either C_S or C_T vanish, were investigated in detail. It is shown there that when $n \gtrsim 2$, the threshold for oscillatory instability is markedly changed from the classical problem, with oscillations at small horizontal scales becoming the favoured mode of convection. Indeed, in the case that the salinity gradient is destabilising and the temperature gradient stabilising (i.e. the fingering regime), oscillations can be preferred even though they are not possible in the classical case.

The question then arises as to the situation when C_S and C_T are both non-zero. It is important to understand whether the scaling laws revealed in HPE21 are typical of this more general case, and also to discover whether new phenomena can occur for particular values of the ratio C_T/C_S, with C_T and C_S both being small. Thus, we revisit the stability problem in the more general case in which C_S and C_T are both non-zero but small, and investigate the effect of changing the ratio between them. As in HPE21, we consider the distinguished limit with $C \ll 1$, $Rs \sim C^{-n}$; it is important to note that such a distinguished limit is very different from the case of $C \to 0$ with all other parameters fixed.

The analysis in the general case turns out to be more challenging than in HPE21: the dispersion relation for the growth rate is now fifth order, and untangling the wavenumber dependence of the preferred modes of instability is more involved. Nonetheless, analytical progress can be made in general when n is sufficiently large. We find a variety of behaviours as the ratio C_S/C_T is varied. In some cases, the endpoint analysis of HPE21 gives a good guide to the behaviour in the more general case. However, we have also identified novel results completely unrelated to those of HPE21; of particular note is the anomalous behaviour of the critical values of Ra and the wavenumber when $C_S/\kappa_S = C_T/\kappa$ (i.e. $\tau_T = \tau_S$).

The layout of the paper is as follows. In § 2 we set out the governing equations and derive the fifth-order dispersion relation that determines the stability boundary. Sections 3 and 4 investigate respectively the nature of this boundary in the first quadrant of the (Rs, Ra) plane $(Rs, Ra > 0)$ and the third quadrant $(Rs, Ra < 0)$. Within both §§ 3 and 4, behaviour for $n \lesssim 2$ is considered before the more extreme (and more analytically tractable) situation where $n \gtrsim 3$. The anomalous region where $C_S/\kappa_S \approx C_T/\kappa$ in the first quadrant is treated in detail in § 3; in the third quadrant we find that steady convection is preferred, as shown in § 4. In § 5 we investigate the growth rates of unstable modes beyond the stability boundary. We conclude in § 6 with a discussion of the results and prospects for future work.

2. Mathematical formulation

2.1. *Maxwell–Cattaneo diffusion*

To derive the governing equations, it is necessary to consider the modifications from the M–C effect to be expected in an incompressible fluid moving with velocity $\boldsymbol{u}$. As in HPE21, in which further details may be found, here we follow the formulation of Christov (2009), which leads to the equation

$$\tau_T \left[\frac{\partial Q_T}{\partial t} + \boldsymbol{\nabla} \cdot (\boldsymbol{u}\, Q_T) \right] = -Q_T - K \nabla^2 T, \tag{2.1}$$

https://doi.org/10.1017/jfm.2026.11340 Published online by Cambridge University Press

where Q_T is the divergence of the heat flux and where we have assumed that K is constant. As $\boldsymbol{u}$ is incompressible, the left-hand side of (2.1) can be written as the usual Lagrangian derivative of Q_T. The equation for the salt flux may be obtained, analogously, as

$$\tau_S \left[\frac{\partial Q_S}{\partial t} + \boldsymbol{\nabla} \cdot (\boldsymbol{u}\, Q_S) \right] = -Q_S - \kappa_S \nabla^2 S. \tag{2.2}$$

We note that the relation between salt flux and salt concentration differs from that between heat flux and temperature; hence the appearance of K in (2.1) but κ_S in (2.2).

2.2. *Governing equations*

As in HPE21, we consider a horizontal layer of an incompressible (Boussinesq) viscous M–C fluid, initially at rest, contained between two planes at $z = 0$ (bottom) and $z = d\pi$ (top). The fluid has kinematic viscosity ν, and thermal and salt diffusivities κ, κ_S. The density depends linearly on two components that diffuse at different rates. In equilibrium, the fluid is at rest, with temperature and salinity differences across the layer of ΔT and ΔS. The basic state temperature and salinity, $\overline{T}$ and $\overline{S}$, are thus given by

$$\overline{T} = T_0 + \Delta T(1 - z/d\pi), \qquad \overline{S} = S_0 + \Delta S(1 - z/d\pi), \tag{2.3}$$

where T_0 and S_0 are representative values of temperature and salinity. For the perturbed state, with velocity $\boldsymbol{u} = (u, v, w)$, we express the temperature and salinity by $T = \overline{T} + \widehat{T}$, $S = \overline{S} + \widehat{S}$. The density ρ of the fluid obeys a linear relation of the form

$$\rho = \rho_0 \left(1 - \alpha_T \left(T - T_0\right) + \alpha_S \left(S - S_0\right)\right), \tag{2.4}$$

where $\rho_0 = \rho(T_0, S_0)$, and α_T and α_S are (constant) coefficients of expansion. The crucial difference in the governing equations for the M–C system, in comparison with those of classical double-diffusive convection (with no M–C effects), is the replacement of the classical Fick's law equations for T and S by the modified equations (2.1) and (2.2). On adopting the standard scalings for distance, time, velocity, heat flux, temperature, salinity flux, salinity and pressure of d, d^2/κ, κ/d, $\Delta T K/d$, ΔT, $\Delta S \kappa_S/d$, ΔS and $\rho_0 \nu \kappa/d^2$, and dropping the hats, the governing equations take the form

$$\frac{1}{\sigma}\frac{D\boldsymbol{u}}{Dt} = -\boldsymbol{\nabla} p + RaT\hat{\boldsymbol{z}} - Rs S\hat{\boldsymbol{z}} + \nabla^2 \boldsymbol{u}, \tag{2.5}$$

$$\boldsymbol{\nabla} \cdot \boldsymbol{u} = 0, \tag{2.6}$$

$$\frac{DT}{Dt} = w - Q_T, \tag{2.7}$$

$$2C_T \frac{DQ_T}{Dt} = -Q_T - \nabla^2 T, \tag{2.8}$$

$$\frac{DS}{Dt} = w - Q_S, \tag{2.9}$$

$$2C_S \frac{DQ_S}{Dt} = -Q_S - \tau \nabla^2 S, \tag{2.10}$$

where the Rayleigh number Ra, the salt Rayleigh number Rs, the Prandtl number σ and the diffusivity ratio τ are defined by

$$Ra = \frac{g\alpha_T \Delta T d^3}{\kappa \nu}, \quad Rs = \frac{g\alpha_S \Delta S d^3}{\kappa \nu}, \quad \sigma = \frac{\nu}{\kappa}, \quad \tau = \frac{\kappa_S}{\kappa}. \tag{2.11}$$

https://doi.org/10.1017/jfm.2026.11340 Published online by Cambridge University Press

With the Rayleigh numbers so defined, positive (negative) Ra is thermally destabilising (stabilising), whereas positive (negative) Rs is solutally stabilising (destabilising).

These governing equations are the same as those derived in HPE21, where we examined the limiting cases of $C_S = 0$ and $C_T = 0$. Our aim here is to understand the nature of any instability in between these two limits. Thus, rather than working with C_T and C_S directly, it is instructive to define two new parameters:

$$\Gamma = C_S + C_T, \qquad \lambda = \frac{C_S - C_T}{C_S + C_T}. \tag{2.12}$$

For certain parts of the analysis, it is also convenient to work with the quantities

$$\lambda_1 = \frac{C_S}{\Gamma} = \frac{1}{2}(1+\lambda), \qquad \lambda_2 = \frac{C_T}{\Gamma} = \frac{1}{2}(1-\lambda), \qquad \alpha = \frac{Cs}{C_T} = \frac{\lambda_1}{\lambda_2}. \tag{2.13}$$

We shall be interested in the case of $\Gamma \ll 1$ (i.e. C_T and C_S both small); λ varies between -1 ($C_S = 0$) and $+1$ ($C_T = 0$).

2.3. *Linearisation and stability considerations*

As in HPE21, we address the linear stability of the basic state given by (2.3) and (2.4), subject to the standard boundary conditions in which the horizontal boundaries are impermeable and stress-free, and on which the temperature and salinity are fixed. Thus,

$$\frac{\partial u_x}{\partial z} = \frac{\partial u_y}{\partial z} = u_z = T = S = 0 \quad \text{on} \quad z = 0, \pi, \tag{2.14}$$

noting that z is now dimensionless. We assume periodicity in the horizontal directions. In general, we may decompose the solenoidal velocity as

$$\boldsymbol{u} = \boldsymbol{\nabla} \times \left(\boldsymbol{\nabla} \times \mathcal{P}\hat{\boldsymbol{z}}\right) + \boldsymbol{\nabla} \times \mathcal{T}\hat{\boldsymbol{z}}. \tag{2.15}$$

The linearised form of (2.5) shows, however, that $\mathcal{T}$ decays for all parameter values, and thus only $\mathcal{P}$ is of relevance. Following the usual approach to the classical double-diffusive stability problem, we seek solutions to the linearised versions of (2.5)–(2.10) of the form

$$\mathcal{P} \propto T \propto S \propto Q_T \propto Q_S \propto f(x, y) \sin mz \, \mathrm{e}^{st}, \tag{2.16}$$

where the planform function $f(x, y)$ satisfies

$$\nabla_H^2 f = -k^2 f, \tag{2.17}$$

with ∇_H^2 being the horizontal Laplacian. For the classical problem, with no M–C effects (i.e. $\Gamma = 0$), it is readily shown that the fundamental mode (i.e. $m = 1$) is the most readily destabilised. Here we shall also restrict attention to the $m = 1$ mode, but will discuss this assumption in § 6, in light of the results.

On substitution from (2.16) into the linearised forms of (2.5)–(2.11), we obtain, after some algebraic manipulation, a quintic dispersion relation for the growth rate s:

$$a_5 s^5 + a_4 s^4 + a_3 s^3 + a_2 s^2 + a_1 s + a_0 = 0, \tag{2.18}$$

https://doi.org/10.1017/jfm.2026.11340 Published online by Cambridge University Press

where

$$a_5 = \frac{\Gamma^2(1-\lambda^2)\beta^2}{\sigma}, \tag{2.19a}$$

$$a_4 = \frac{2\Gamma}{\sigma}\beta^2 + \Gamma^2(1-\lambda^2)\beta^4, \tag{2.19b}$$

$$a_3 = \frac{\beta^2}{\sigma} + \frac{\Gamma}{\sigma}\left(1+2\sigma+\tau+\lambda(1-\tau)\right)\beta^4 + \Gamma^2(1-\lambda^2)\left(Rs-Ra\right)k^2, \tag{2.19c}$$

$$a_2 = \left(1+\frac{1+\tau}{\sigma}\right)\beta^4 + \Gamma\left(1+\tau+\lambda(1-\tau)\right)\beta^6 + 2\Gamma\left(Rs-Ra\right)k^2, \tag{2.19d}$$

$$a_1 = \left(1+\tau+\frac{\tau}{\sigma}\right)\beta^6 + Rs\left(1+\Gamma(1+\lambda)\beta^2\right)k^2 - Ra\left(1+\tau\Gamma(1-\lambda)\beta^2\right)k^2, \tag{2.19e}$$

$$a_0 = \tau\beta^8 + Rs\beta^2k^2 - \tau Ra\beta^2k^2, \tag{2.19f}$$

with $\beta^2 = k^2+1$. As shown in HPE21, the symmetry of the system allows us to consider only the case of $\tau < 1$.

In this paper, we shall concentrate on determining the conditions for the onset of instability; this may occur either as a direct mode (steady convection), in which case the growth rate s passes through zero, or as an oscillatory mode, in which case, at onset, $s = \pm i\omega$, with $\omega \in \mathbb{R}_+$. It is traditional in studies of double-diffusive convection to treat Ra as the bifurcation parameter, although, mathematically, there is nothing to favour Ra over Rs. For comparison with the existing literature, we shall maintain this tradition here. We shall denote $Ra(k^2)$ at the onset of steady (oscillatory) convection by $Ra^{(s)}$ ($Ra^{(o)}$), the minimum of $Ra^{(s)}$ ($Ra^{(o)}$) over all wavenumbers as $Ra_c^{(s)}$ ($Ra_c^{(o)}$), the associated value of k^2 by k_{sc}^2 (k_{oc}^2), and, for the case of oscillatory onset, the associated value of ω^2 by ω_c^2. The lesser of $Ra_c^{(s)}$ and $Ra_c^{(o)}$ is the overall critical Rayleigh number, which we denote by Ra_c, with $k^2 = k_c^2$. We shall refer to the mode that first becomes unstable as Ra is increased as the preferred or favoured mode.

From the form of the flux equations (2.8) and (2.10) it is clear that M–C effects occur only in time-derivative terms, so these effects have no influence on the onset of steady convection. The value of Ra at the onset of steady convection is therefore given by

$$Ra = Ra^{(s)} = \frac{Rs}{\tau} + \frac{\beta^6}{k^2}. \tag{2.20}$$

Since β^6/k^2 is minimised when $k^2 = 1/2$,

$$Ra_c^{(s)} = \frac{Rs}{\tau} + \frac{27}{4}. \tag{2.21}$$

To determine the onset of oscillatory instability, we set $s = \pm i\omega$, with $\omega \in \mathbb{R}_+$, leading to the coupled equations

$$a_5\omega^4 - a_3\omega^2 + a_1 = 0, \qquad a_4\omega^4 - a_2\omega^2 + a_0 = 0. \tag{2.22a,b}$$

Since Ra and Rs occur linearly in coefficients a_0, a_1, a_2, a_3 – and are absent in a_4 and a_5 – we can combine equations (2.22) to derive a cubic equation for ω^2 that does not involve Ra (or, alternatively, Rs), or eliminate ω^2 to derive an expression cubic in Ra and Rs. In HPE21 the corresponding expressions were quadratic rather than cubic, and we made use of each. Here the expressions for the coefficients of the cubic in Ra are extremely lengthy,

https://doi.org/10.1017/jfm.2026.11340 Published online by Cambridge University Press

and so, with one exception, our primary mode of attack will be via the cubic equation for ω^2, which takes the form

$$b_6\omega^6 + b_4\omega^4 + b_2\omega^2 + b_0 = 0, \tag{2.23}$$

where

$$b_6 = \sigma\Gamma^4\big(1-\lambda^2\big)^2\beta^2, \tag{2.24a}$$

$$b_4 = \Gamma^2\big(2\sigma(1+\lambda^2) + (1+\lambda)^2\big)\beta^2 - \sigma\Gamma^3(1-\lambda^2)\big(1+2\tau+\lambda(1-2\tau)\big)\beta^4, \tag{2.24b}$$

$$\begin{aligned} b_2 = {} & (1+\sigma)\beta^2 - \Gamma\big(\sigma + 2\tau(1+\sigma) + \lambda(2\tau(1+\sigma)-\sigma)\big)\beta^4 \\ & + \sigma\Gamma^2\big((\tau-1)\lambda^2 - 2(1+\tau)\lambda + \tau - 1\big)Rsk^2, \end{aligned} \tag{2.24c}$$

$$+ \sigma\tau\Gamma^2\big((\tau-2)\lambda^2 - 2\tau\lambda + 2 + \tau\big)\beta^6, \tag{2.24d}$$

$$b_0 = \tau^2(1+\sigma)\beta^6 - \Gamma(1-\lambda)\sigma\tau^2\beta^8 - \sigma(1-\tau)Rsk^2 + 2\sigma\tau\Gamma\lambda Rs\beta^2k^2. \tag{2.24e}$$

For completeness, the cubic equation determining $Ra^{(o)}$ is contained in the supplementary material.

We recap briefly the results for the classical double-diffusive problem; more details can be found in HPE21. Oscillatory instability can occur only in the first quadrant of the (Rs, Ra) plane (i.e. Rs and Ra both positive); this is often referred to as the diffusive regime. The marginal value of Ra for oscillatory motions (i.e. when $s = \pm i\omega$, $\omega \in \mathbb{R}_+$) is given by

$$Ra^{(o)} = \left(\frac{\sigma+\tau}{1+\sigma}\right)Rs + \frac{(1+\tau)(\sigma+\tau)}{\sigma}\frac{\beta^6}{k^2}, \tag{2.25}$$

provided also that $\omega^2 > 0$, which translates to the condition

$$Rs > \frac{\tau^2(1+\sigma)}{\sigma(1-\tau)}\frac{\beta^6}{k^2}. \tag{2.26}$$

It follows from (2.26) that oscillatory motions are preferred at onset provided that

$$Rs > \frac{27}{4}\frac{\tau^2(1+\sigma)}{\sigma(1-\tau)}; \tag{2.27}$$

from (2.25), the critical Rayleigh number for oscillatory convection is then given by

$$Ra_c^{(o)} = \left(\frac{\sigma+\tau}{1+\sigma}\right)Rs + \frac{27(1+\tau)(\sigma+\tau)}{4\sigma}. \tag{2.28}$$

In the third quadrant (i.e. $Rs < 0$, $Ra < 0$), instability always occurs as steady convection, with the critical Rayleigh number given by (2.21); this is typically referred to as the salt fingering regime.

In HPE21 we studied the role of the (small) M–C effects by considering different regimes for (large) Rs; this was achieved by scaling Rs with either C_T^{-n} (for $C_S = 0$) or C_S^{-n} (for $C_T = 0$) and investigating the nature of the behaviour with increasing n. In a similar vein, for the more general problem considered here, it is instructive to consider the regimes defined by $Rs = O(\Gamma^{-n})$. As discussed above, in the classical problem, it is in the first and third quadrants of the (Rs, Ra) plane that double-diffusive effects come into play (in the second quadrant the fluid is top heavy, and hence unstable to overturning, whereas the fourth quadrant is a region of stability). Thus, with the inclusion of M–C

https://doi.org/10.1017/jfm.2026.11340 Published online by Cambridge University Press

effects, we examine separately the behaviour in the first and third quadrants in the $(Rs,\ Ra)$ plane.

3. The first quadrant: $Rs > 0$, $Ra > 0$

3.1. $0 < n \leqslant 1$

When Rs assumes $O(1)$ values, the problem is essentially that of classical double-diffusive convection. Qualitative changes from the classical problem first arise when $n = 1$; to investigate this regime, we rescale both Rayleigh numbers with Γ^{-1}. For classical double diffusion, the critical wavenumber for oscillatory convection (and indeed steady convection also) is given by $k^2 = 1/2$. To explore how the M–C effect can influence this picture, we consider the regime $\Gamma \ll 1$, $Rs = \Gamma^{-1}\widetilde{Rs}$, $Ra = \Gamma^{-1}\widetilde{Ra}$, where $\widetilde{Rs}$ and $\widetilde{Ra}$ are $O(1)$, and with $k = O(1)$. The details of the associated analysis, which is in the same spirit as for the endpoints $\lambda = \pm 1$, though algebraically more messy, are contained in Appendix A. The leading-order expression for the onset of oscillatory convection ($\widetilde{Ra}_0$) is given by (A3), namely

$$\widetilde{Ra}_0 = \frac{(\sigma+\tau)}{(1+\sigma)}\widetilde{Rs} \qquad \text{or} \qquad Ra_0 = \frac{(\sigma+\tau)}{(1+\sigma)}Rs. \tag{3.1}$$

We note that $\widetilde{Ra}_0$ is independent of both λ and k. Determination of the critical wavenumber comes at the next order (i.e. determining $\widetilde{Ra}_1$), where $\mathrm{d}\widetilde{Ra}_1/\mathrm{d}k^2 = 0$ gives rise to a quintic polynomial in k^2 (expression (A6), with coefficients (A5)). Figure 1(*a–c*) shows the evolution of the real parts of the roots of the quintic polynomial (A6) as $\widetilde{Rs}$ is increased for three values of λ. With $Rs = 0$, the only real positive root is at $k = 1/2$ (the classical case). For all values of λ, the existing mode moves to higher k. As for $C_S = 0$ (i.e. $\lambda = -1$), for λ close to -1, two equal stationary points appear at a critical value of Rs (Rs^*, say), which then separate with a further increase in Rs; k^2 remains negative (and thus unphysical) for the other two roots (see figure 1*a*). As λ increases, Rs^* increases (it has moved off to the right in figure 1*b*), with $Rs^* \to \infty$ as $\lambda \to \lambda^*$, where

$$\lambda^* = \frac{\sqrt{\sigma+\tau} - \sqrt{\tau(1+\sigma)}}{\sqrt{\sigma+\tau} + \sqrt{\tau(1+\sigma)}}. \tag{3.2}$$

For $\lambda > \lambda^*$, there is only one real stationary point (as in figure 1*c*). Thus, for $-1 \leqslant \lambda < \lambda^*$, the M–C influence is felt for $Rs = O(\Gamma^{-1})$ by the emergence of two new stationary points in the oscillatory stability boundary. More generally, it can be seen that, for all λ, there is a shift of the classical mode to higher wavenumbers. Figure 1(*d–f*) shows the oscillatory stability boundary with no approximations (calculated numerically), together with the zeroth-order approximation $\widetilde{Ra}_0$, and with the first-order correction $\widetilde{Ra}_1$; the latter is essentially indistinguishable from the boundary of the full system. The oscillatory stability boundary for the classical problem, given by (2.25), is also shown. The three stationary points in figure 1(*d*) correspond to the three positive roots for k^2 at $\widetilde{Rs} = 15$ in figure 1(*a*). Whenever there is more than one minimum in the $Ra^{(o)}$ vs k^2 curve (as in figure 1*d*), the higher wavenumber mode is always preferred. We note also that since $Ra_c^{(s)} \approx Rs/\tau > Ra_0$ (from (2.21)), the preferred mode is always oscillatory.

3.2. $n = 2$

It is helpful to begin by summarising the main findings from HPE21 of the $n = 2$ regime for $\lambda = \pm 1$. When $\lambda = -1$ ($C_S = 0$), Ra, as a function of k^2, has two minima: a large wavelength mode with $k^2 = O(C_T)$ and a small wavelength mode with $k^2 = O(C_T^{-1})$.

https://doi.org/10.1017/jfm.2026.11340 Published online by Cambridge University Press

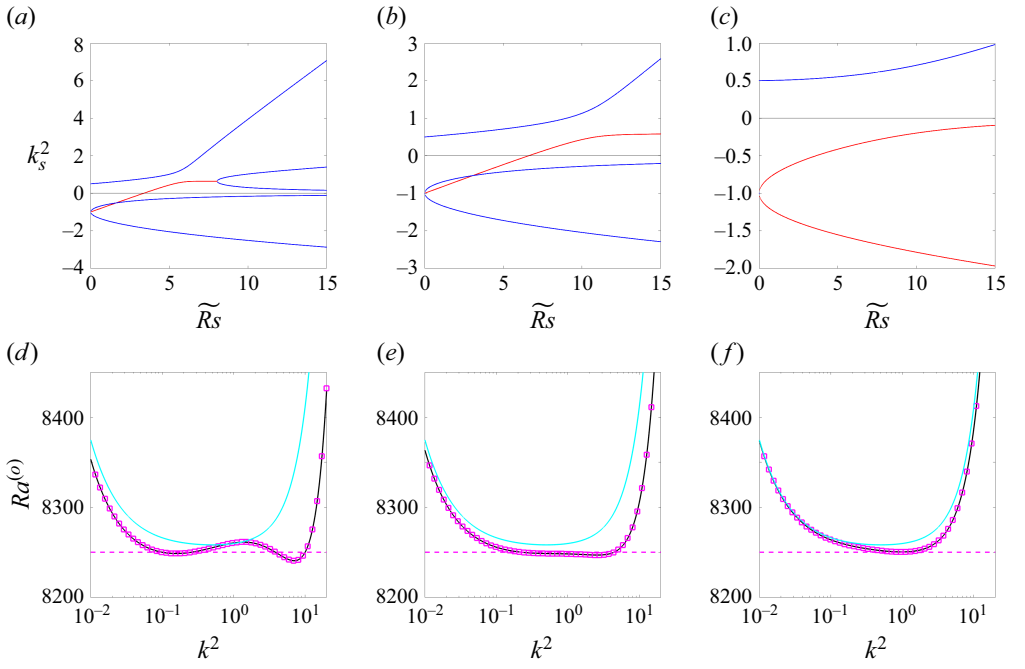


Figure 1. (*a–c*) The real parts of the roots of (A6) for k_s^2 as a function of $\widetilde{Rs}$ for $0 < n \leqslant 1$; blue lines denote real roots, the red line denotes the real part of a conjugate pair; $\sigma = 1$, $\tau = 0.1$, with (*a*) $\lambda = -0.8$, (*b*) $\lambda = 0$, (*c*) $\lambda = 0.8$. (*d–f*) Corresponding plots of the oscillatory stability boundary (grey solid line), together with the zeroth-order asymptotic expression (A3) (magenta dashed line) and the first-order correction (A5) (magenta squares); for the numerical results, $\Gamma = 10^{-3}$, $Rs = 1.5 \times 10^4$ (corresponding to $\widetilde{Rs} = 15$). For comparison, the cyan line shows $Ra^{(o)}$ for the classical problem, given by (2.25).

The $k^2 = O(C_T^{-1})$ mode is always preferred; the onset of instability is oscillatory, with $Ra_c = O(C_T^{-2})$. When $\lambda = 1$ ($C_T = 0$), there is only one minimum of Ra as a function of wavenumber, with $k^2 = O(C_S^{-1/2})$; the onset of instability is oscillatory, with $Ra_c = O(C_S^{-2})$. Even for the limiting cases of $\lambda = \pm 1$, analytical progress in the $n = 2$ regime was limited, since the only simplification is that (at high wavenumbers) $\beta^2 \approx k^2$. For $-1 < \lambda < 1$, where the behaviour is more complex, the $n = 2$ regime is essentially accessible only to numerical study.

Figure 2 shows $Ra^{(o)}$ as a function of k^2 for a large and small value of σ ($\sigma = 10$ in panels *a–c* and $\sigma = 0.1$ in panels *d–f*), with $\tau = 0.5$, and for $\lambda = -0.8, 0, 0.8$; for comparison, the limiting values of $\lambda = -1$ and $\lambda = 1$ are also shown, respectively, on the $\lambda = -0.8$ and $\lambda = 0.8$ plots. Note that since $Ra_c^{(s)} \approx Rs/\tau = 2 \times 10^6$, the oscillatory mode is preferred, and hence determines the overall stability boundary. For both values of σ, the qualitative behaviour as λ changes is the same. For $\lambda = -0.8$, there are two minima in $Ra^{(o)}$, as for $\lambda = -1$; the preferred mode is at the larger wavenumber, with $k^2 = O(C_T^{-1})$. As λ increases, the (non-preferred) minimum at small k^2 disappears and the preferred mode moves gradually to smaller k^2. The minima of the $\lambda = 0.8$ curves are located at slightly larger values of k^2 than those at $\lambda = 1$, where the preferred mode has $k^2 = O(C_S^{-1/2})$. For comparison, $Ra^{(o)}$ for the classical problem, given by (2.25), is also shown in figure 2; for the cases illustrated, it can be seen that the M–C effect is a destabilising influence.

https://doi.org/10.1017/jfm.2026.11340 Published online by Cambridge University Press

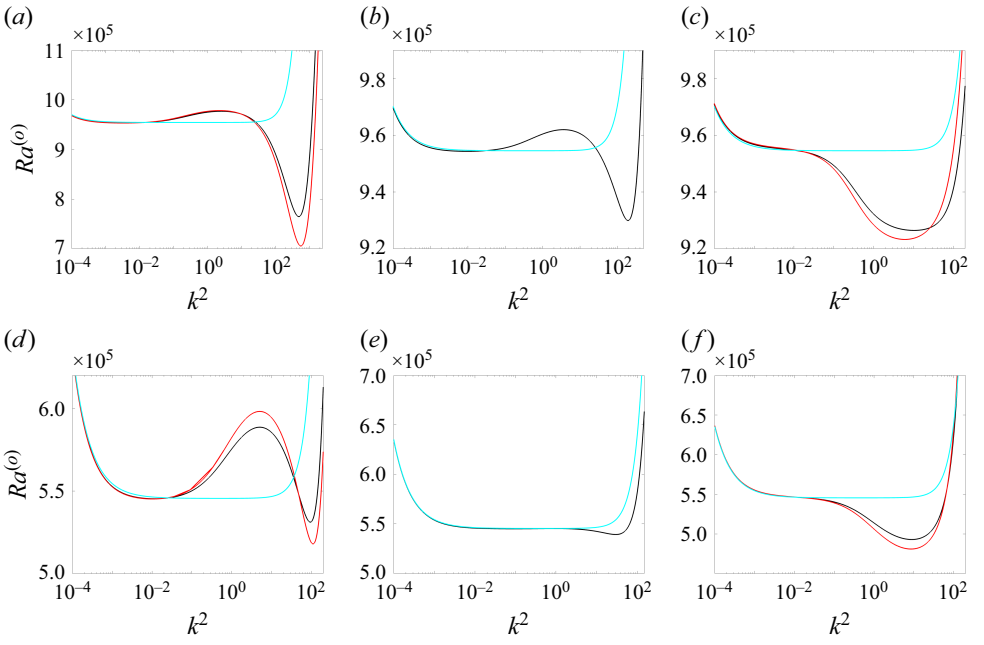


Figure 2. Plots of $Ra^{(o)}$ versus k^2 for $\Gamma = 10^{-3}$, $Rs = 10^6$ ($n = 2$), $\tau = 0.5$. In (*a–c*), $\sigma = 10$, with (*a*) $\lambda = -0.8$ (black), $\lambda = -1$ (red); (*b*) $\lambda = 0$; (*c*) $\lambda = 0.8$ (black), $\lambda = 1$ (red). In (*d–f*), $\sigma = 0.1$, with (*d*) $\lambda = -0.8$ (black), $\lambda = -1$ (red); (*e*) $\lambda = 0$; (*f*) $\lambda = 0.8$ (black), $\lambda = 1$ (red). The cyan lines show $Ra^{(o)}$ for the classical problem, given by (2.25).

Figure 3 shows $Ra_c^{(o)}$, k_c^2 and ω_c^2 as a function of λ for four pairs of (σ, τ) values. Again, $Ra_c^{(s)} \approx Rs/\tau$ exceeds $Ra_c^{(o)}$ and so the oscillatory stability boundary determines the overall boundary. As shown in HPE21, at both endpoints ($\lambda = \pm 1$), $Ra_c^{(o)} = O(\Gamma^{-2})$, though which of these is the more unstable depends on the values of σ and τ (contrast, for example, figures 3*a* and 3*d*). In the displayed numerical results, the most stable configuration has a mid-range value of λ. However, at very large σ (not shown) and small values of τ, $Ra_c^{(o)}$ essentially increases monotonically with λ over the entire interval; furthermore, for very large σ and τ close to unity, $Ra_c^{(o)}$ increases for $-1 < \lambda \lesssim 0$ and then exhibits very little change over the range $0 \lesssim \lambda < 1$. As already noted, the values of k_c^2 at the endpoints are asymptotically distinct. Thus, there is inevitably a decrease in k_c^2 from $\lambda = -1$ to $+1$; this may or may not be monotonic, depending on the values of σ and τ. Conversely, the frequencies at $\lambda = \pm 1$ both scale as $\omega_c^2 = O(\Gamma^{-2})$, a scaling that is maintained throughout the range of λ. Figure 3 also shows $Ra_c^{(o)}$ for the classical problem, given by (2.28). It can be seen that for the cases illustrated, the M–C effect, save possibly for a small interval of λ, is destabilising.

3.3. $n \geqslant 3$

Figure 4 shows $Ra_c^{(o)}$, k_c^2 and ω_c^2 as functions of λ for $n = 3$, 4, 5. The most striking feature of the $n \geqslant 3$ regime is the appearance of a narrow region close to $\lambda_1/\lambda_2 = \tau$ (or $\lambda = \lambda_d = (\tau - 1)/(\tau + 1)$) in which both the critical wavenumber and its associated frequency are markedly smaller than at nearby values of λ. This region corresponds to $\tau_T = \tau_S$, as discussed in § 1, and we refer to it as 'the dip'. The sharp minima in k_c^2 and ω_c^2

https://doi.org/10.1017/jfm.2026.11340 Published online by Cambridge University Press

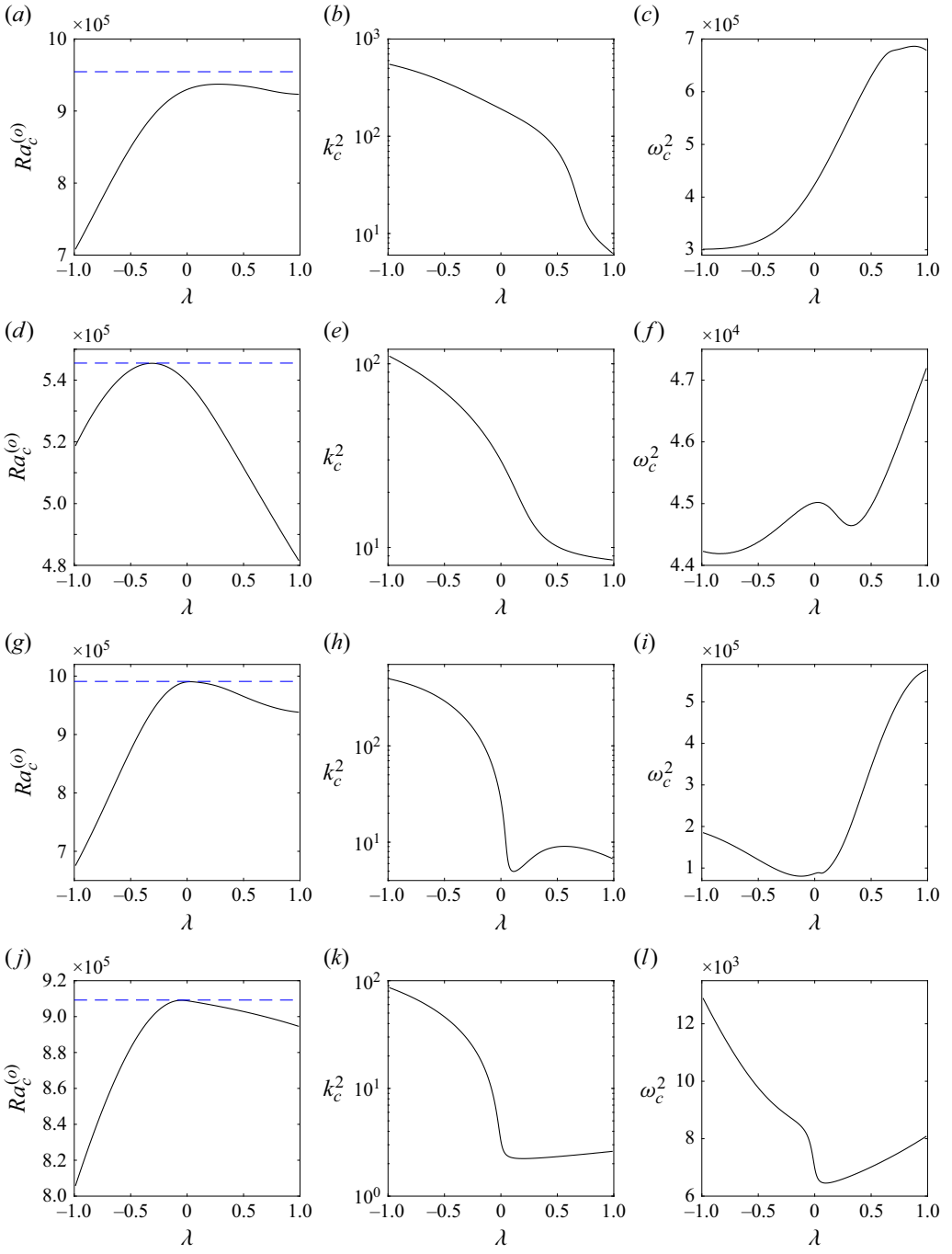


Figure 3. Plots of $Ra_c^{(o)}$, k_c^2 and ω_c^2 versus λ for $\Gamma = 10^{-3}$, $Rs = 10^6$ ($n = 2$). In (a–c), $\sigma = 10$, $\tau = 0.5$; in (d–f), $\sigma = 0.1$, $\tau = 0.5$; in (g–i), $\sigma = 10$, $\tau = 0.9$; in (j–l), $\sigma = 0.1$, $\tau = 0.9$. The blue dashed line shows $Ra_c^{(o)}$ for the classical problem, given by (2.28).

https://doi.org/10.1017/jfm.2026.11340 Published online by Cambridge University Press

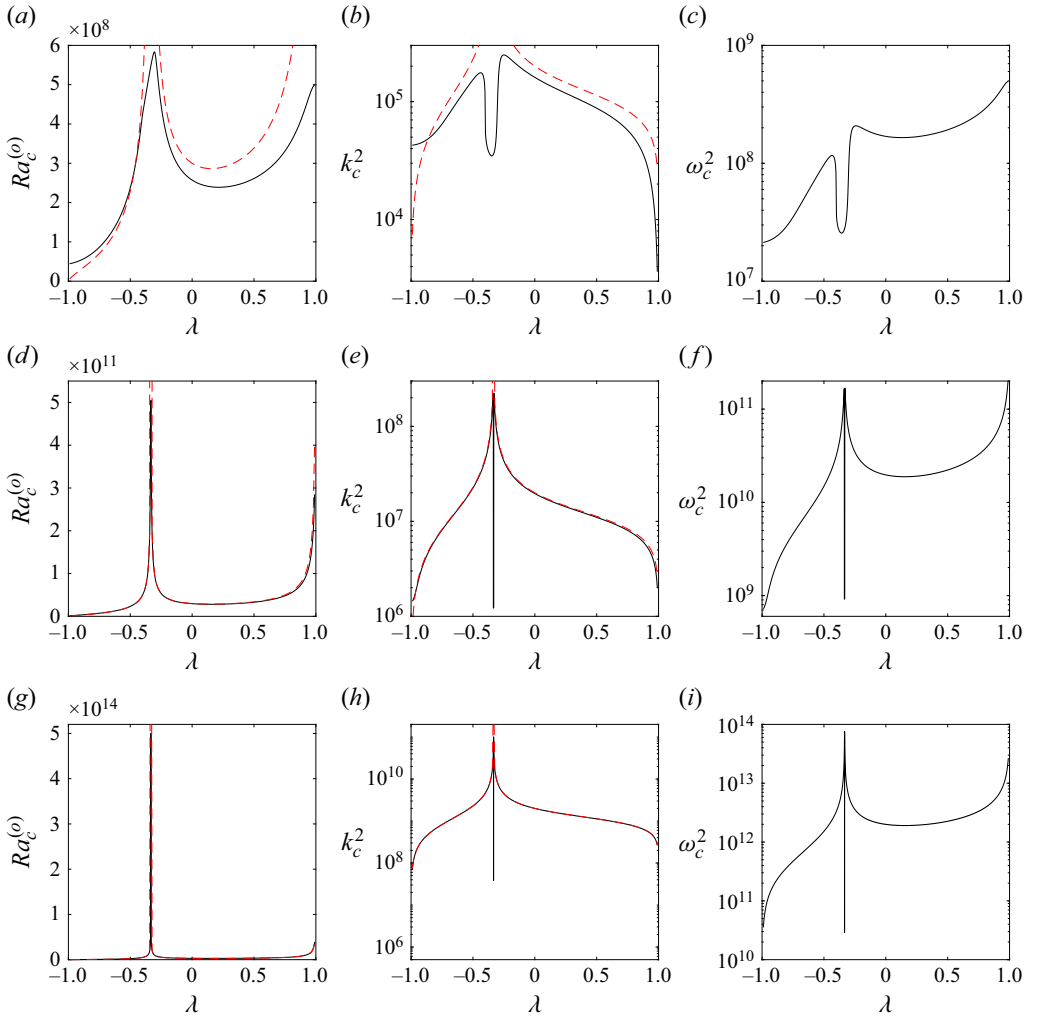


Figure 4. Plots of $Ra_c^{(o)}$, k_c^2 and ω_c^2 versus λ for $\Gamma = 10^{-3}$, $\sigma = 1$, $\tau = 0.5$. In (*a–c*), $Rs = 10^9$ ($n = 3$); in (*d–f*), $Rs = 10^{12}$ ($n = 4$); in (*g–i*), $Rs = 10^{15}$ ($n = 5$). The asymptotic results (3.11) are marked as dashed red lines.

are accompanied by a sharp maximum in $Ra_c^{(o)}$. The analysis below shows that the width of the narrow region is $O(\Gamma^{(n-2)/2})$, as can be seen in figure 5, which shows a small range of λ near λ_d. Figure 6 shows $Ra_c^{(o)}$ as a function of k^2 for values of λ just to the left of the dip, in the dip itself, and just to the right of the dip. The transition of k_c^2 and ω_c^2 in the dip is discontinuous: as λ increases through λ_d, the minimum at larger k^2 (figure 6*a*, with $k_c^2 = 1.77 \times 10^8$) becomes higher than that at smaller k^2, leading to a discontinuous change in the critical wavenumber (figure 6*b*, with $k_c^2 = 1.22 \times 10^6$), before the minimum at large k^2 reasserts itself (figure 6*c*, with $k_c^2 = 2.22 \times 10^8$).

3.3.1. *Asymptotics for general* λ

We can give accurate asymptotic descriptions of the behaviour of the marginal curves in the first quadrant when $\Gamma \ll 1$ and $n \gtrsim 3$ (the larger the value of n the more accurate the results). To begin with, we consider the general case away from the dip, so that λ_1/λ_2 is

https://doi.org/10.1017/jfm.2026.11340 Published online by Cambridge University Press

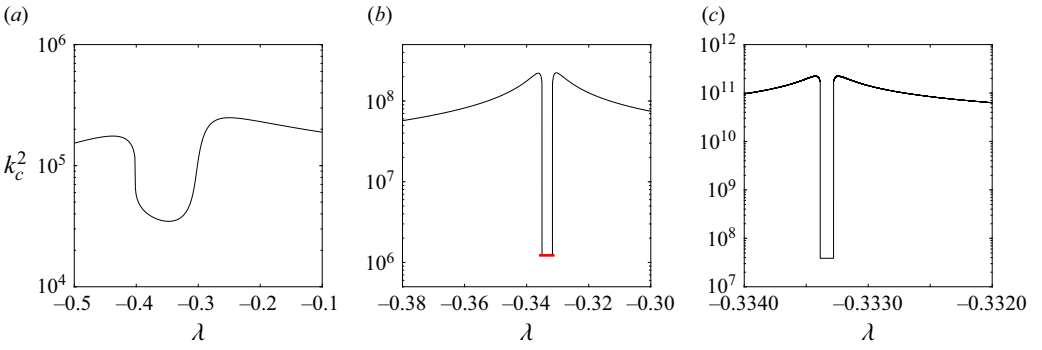


Figure 5. Plots of k_c^2 versus λ, for a restricted range of λ, with $\Gamma = 10^{-3}$, $\sigma = 1$, $\tau = 0.5$. In (a), $Rs = 10^9$ $(n = 3)$; in (b), $Rs = 10^{12}$ $(n = 4)$; in (c), $Rs = 10^{15}$ $(n = 5)$. In (b) the asymptotic result (3.25) is marked as a red line.

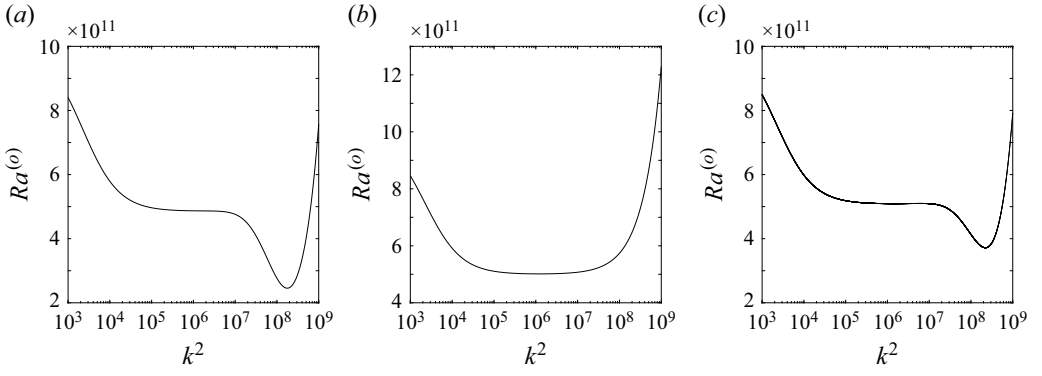


Figure 6. Plots of $Ra^{(o)}$ versus k^2 with $\Gamma = 10^{-3}$, $Rs = 10^{12}$ $(n = 4)$, $\sigma = 1$, $\tau = 0.5$. In (a), $\lambda = -0.34$ (just to the left of the dip); in (b), $\lambda = -0.3335$ (in the middle of the dip); in (c), $\lambda = -0.33$ (just to the right of the dip).

not close to τ. Guided by the numerical results, we pose the following scalings:

$$Rs = \Gamma^{-n}\widetilde{Rs}, \quad k^2 = \Gamma^{(1-2n)/3}\tilde{k}^2, \quad Ra^{(o)} = \Gamma^{-(2+2n)/3}\widetilde{Ra}, \\ \omega^2 \sim k^2/2\Gamma = \Gamma^{-(2+2n)/3}\tilde{\omega}^2. \tag{3.3}$$

Note that $Ra_c^{(o)}$ determined under the scalings (3.3) will be asymptotically smaller than $Ra_c^{(o)}$ for the classical problem (in which, from (2.28), $Ra_c^{(o)}$ and Rs are of the same order).

When $n > 2$, we can define the small parameter $\varepsilon = \Gamma^{(n-2)/3}$. We then make an expansion in powers of ε, with the expansion carried as far as $\varepsilon^2 = \Gamma^{(2n-4)/3}$. Since k^2 is assumed large, we can replace $\beta^2 = k^2 + 1$ by k^2, since the error in doing this is $O(\Gamma^{(2n-1)/3}) = O(\Gamma\varepsilon^2)$.

The leading terms in (2.23) suggest the ansatz

$$\omega^2 = \frac{1}{\lambda_2}\left(\frac{\tilde{k}^2}{2} + \varepsilon p_1 + \varepsilon^2 p_2\right)\Gamma^{-(2+2n)/3}. \tag{3.4}$$

On substituting expression (3.4) into (2.23), we find, correct to $O(\varepsilon^2)$, that

$$b_6\omega^6 = 2\sigma\lambda_1^2\lambda_2^{-1}\left(\tilde{k}^8 + 6\varepsilon p_1\tilde{k}^6 + 12\varepsilon^2 p_1^2\tilde{k}^4 + 6\varepsilon^2 p_2\tilde{k}^6\right)\Gamma^{(7-8n)/3}, \tag{3.5a}$$

https://doi.org/10.1017/jfm.2026.11340 Published online by Cambridge University Press

$$b_4\omega^4 = \Big(-2\sigma\big(\lambda_1^2\lambda_2^{-1} + 2\tau\lambda_1\big)\tilde{k}^8 - 8\varepsilon\sigma\big(\lambda_1^2\lambda_2^{-1} + 2\tau\lambda_1\big)p_1\tilde{k}^6 + \varepsilon^2\big(\sigma + (1+\sigma)\lambda_1^2\lambda_2^{-2}\big)\tilde{k}^6 - 8\varepsilon^2\sigma\big(\lambda_1^2\lambda_2^{-1} + 2\tau\lambda_1\big)\big(p_2\tilde{k}^2 + p_1^2\tilde{k}^4\big)\Big)\,\Gamma^{(7-8n)/3}, \tag{3.5b}$$

$$b_2\omega^2 = \Big(2\sigma\tau(\tau\lambda_2 + 2\lambda_1)\tilde{k}^8 + \varepsilon\big(2\sigma\big(\tau\lambda_2 - \lambda_1^2\lambda_2^{-1}\big)\widetilde{Rs}\tilde{k}^4 + 4\sigma\tau(\tau\lambda_2 + 2\lambda_1)p_1\tilde{k}^6\big) + \varepsilon^2\Big(4\sigma\tau(\tau\lambda_2 + 2\lambda_1)p_2\tilde{k}^6 + 4\sigma\big(\tau\lambda_2 - \lambda_1^2\lambda_2^{-1}\big)p_1\widetilde{Rs}\tilde{k}^2 - \Big(\sigma + 2\tau\big(1+\sigma\big)\lambda_1\lambda_2^{-1}\Big)\tilde{k}^6\Big)\Big)\,\Gamma^{(7-8n)/3}, \tag{3.5c}$$

$$b_0 = \Big(-2\sigma\tau^2\lambda_2\tilde{k}^8 + 2\varepsilon\sigma\tau(\lambda_1 - \lambda_2)\widetilde{Rs}\tilde{k}^4 + \varepsilon^2\tau^2(1+\sigma)\tilde{k}^6\Big)\,\Gamma^{(7-8n)/3}. \tag{3.5d}$$

By construction, the leading-order terms in (2.23) cancel. At $O(\varepsilon)$ we find that

$$p_1 = \frac{\lambda_1\widetilde{Rs}}{2(\lambda_1 - \tau\lambda_2)\tilde{k}^2}, \tag{3.6}$$

and at $O(\varepsilon^2)$ we obtain

$$16p_1^2\sigma\left(\lambda_1^2\lambda_2^{-1} - \tau\lambda_1\right)\tilde{k}^4 + \left(4p_2\sigma\lambda_2^{-1} + (1+\sigma)\lambda_2^{-2}\right)(\lambda_1 - \tau\lambda_2)^2\,\tilde{k}^6 + 4p_1\sigma\lambda_2^{-1}\left(\tau\lambda_2^2 - \lambda_1^2\right)\widetilde{Rs}\tilde{k}^2 = 0. \tag{3.7}$$

Finally, substituting for p_1 from (3.6) into (3.7) yields

$$p_2 = -\frac{1}{4}\left(\frac{1+\sigma}{\lambda_2\sigma} + \frac{2\lambda_1\left(\lambda_1^2 + \tau\lambda_2^2\right)\widetilde{Rs}^2}{(\lambda_1 - \tau\lambda_2)^3\,\tilde{k}^6}\right). \tag{3.8}$$

We have now found the expression of ω^2 correct to order ε^2 in expansion (3.4). To determine the corresponding value of the critical Rayleigh number, we substitute for ω^2 into either (2.22*a*) or (2.22*b*); expanding as before and cancelling a common factor of Γ, we obtain the following expressions for the various terms in, for example, (2.22*b*):

$$a_4\omega^4 = \frac{\lambda_1}{\lambda_2}\tilde{k}^8 + 4\varepsilon\frac{\lambda_1}{\lambda_2}p_1\tilde{k}^6 + \varepsilon^2\left(4\frac{\lambda_1}{\lambda_2}(p_2\tilde{k}^6 + p_1^2\tilde{k}^4) + \frac{1}{2\lambda_2^2\sigma}\tilde{k}^6\right), \tag{3.9a}$$

$$a_2\omega^2 = \frac{1}{\lambda_2}\Big[(\tau\lambda_2 + \lambda_1)\tilde{k}^8 + \varepsilon\left(\widetilde{Rs}\tilde{k}^4 + 2(\tau\lambda_2 + \lambda_1)p_1\tilde{k}^6\right) + \varepsilon^2\left(2(\tau\lambda_2 + \lambda_1)p_2\tilde{k}^6 + 2\widetilde{Rs}\,p_1\tilde{k}^2 + \frac{1}{2}\left(\left(1 + \frac{1+\tau}{\sigma}\right)\tilde{k}^6 - 2\widetilde{Ra}\tilde{k}^4\right)\right)\Big], \tag{3.9b}$$

$$a_0 = \tau\tilde{k}^8 + \varepsilon\widetilde{Rs}\tilde{k}^4 - \varepsilon^2\tau\widetilde{Ra}\tilde{k}^4. \tag{3.9c}$$

It is easily checked that both the $O(1)$ and $O(\varepsilon)$ terms in (2.22*b*) cancel; the remaining terms lead to the relatively simple relation

$$\widetilde{Ra} = \frac{\tilde{k}^2}{2\lambda_2} + \frac{\lambda_1^2\widetilde{Rs}^2}{(\tau\lambda_2 - \lambda_1)^2\tilde{k}^4} \Longrightarrow Ra^{(o)} = \frac{\Gamma^{-1}k^2}{2\lambda_2} + \frac{\lambda_1^2Rs^2}{(\tau\lambda_2 - \lambda_1)^2k^4}. \tag{3.10}$$

https://doi.org/10.1017/jfm.2026.11340 Published online by Cambridge University Press

Minimising $Ra^{(o)}$ with respect to k^2 determines the critical values k_c^2 and $Ra_c^{(o)}$ as

$$k_c^2 = \left(\frac{4\lambda_1^2\lambda_2\Gamma Rs^2}{(\tau\lambda_2-\lambda_1)^2}\right)^{\frac{1}{3}}, \qquad Ra_c^{(o)} = \frac{3}{2\lambda_2}\left(\frac{\lambda_1^2\lambda_2\Gamma^{-2}Rs^2}{2(\tau\lambda_2-\lambda_1)^2}\right)^{\frac{1}{3}}. \tag{3.11}$$

The asymptotic results (3.11) are plotted in figure 4. As expected, the agreement with the full system improves with increasing n; for $n=4$ and $n=5$, the asymptotic and numerical results are almost indistinguishable, except in the immediate neighbourhood of the dip, where expressions (3.11) diverge. In each case, the classical stability boundary is at a much higher value of Ra, and so is not shown.

It is interesting to relate the above results to those for $\lambda=\pm1$ obtained in HPE21. From the expression for $Ra_c^{(o)}$ in (3.11) we can calculate the position of the minimum in the Ra vs λ curve, which is at $\lambda=-1+2\sqrt{\tau/(1+\tau)}$. We note that at this minimum, $Ra=O(\Gamma^{-(2+2n)/3})$, whereas, when $\lambda=-1$, different asymptotic scalings apply.

For $\lambda=-1$,

$$Ra \approx \Gamma^{-1}\left(Rs/\tau\right)^{1/2} = O(\Gamma^{-(1+n/2)}); \tag{3.12}$$

hence, the smallest value of $\widetilde{Ra}_c$ always occurs at $\lambda=-1$ ($C_s=0$). How then does the solution approach $\lambda=-1$? Assuming that the full solution varies slowly with λ near $\lambda=-1$, we can estimate where the internal solution given by (3.11) attains the 'left-hand' value. Assuming λ_1 is small (and hence $\lambda_2\approx1$), we find an intersection of the two solutions when $\lambda=-1+\delta\lambda_1$ where

$$\delta\lambda_1 = O\left(\left(Rs/\tau\Gamma^2\right)^{-1/4}\right); \tag{3.13}$$

this is small when $n\gtrsim3$.

Near $\lambda=1$ ($\lambda_2=0$), on the other hand, (3.11) implies that $Ra=O(\Gamma^{-2/3}(Rs/\lambda_2)^{2/3})$ as $\lambda_2\to0$. However, the scaling for $\lambda=1$ gives

$$Ra \approx \sigma Rs/(1+\sigma). \tag{3.14}$$

Matching these two results is accomplished through a boundary layer of thickness $\delta\lambda_2$, where

$$\delta\lambda_2 = O\left((1+\sigma^{-1})^{3/2}(\Gamma^2Rs)^{-1/2}\right). \tag{3.15}$$

3.3.2. *Asymptotics near the dip*

Near the critical value $\lambda_d=(\tau-1)/(\tau+1)$ different asymptotics apply, as can be seen from the numerical results, which give a much lower critical wavenumber. This much smaller wavenumber mode exists for a range of λ, but the analysis is easier when λ is close to λ_d. For the time being, then, we set

$$\lambda_1 = \lambda_2(\tau+\gamma\kappa), \tag{3.16}$$

where we introduce the expansion parameter $\delta=\Gamma^{(n/2-1)}\ll1$ ($n>2$) and write $\gamma=\delta/\lambda_2$. Following numerical evidence, we write $Ra=\Gamma^{-n}\widetilde{Ra}$, $k^2=\Gamma^{-n/2}\tilde{k}^2$ (note that these differ from the scalings in § 3.3.1), and carry our analysis to $O(\delta)$. As in § 3.3.1, since $k^2\gg1$ we would like to approximate $\beta^2=1+k^2$ by k^2. The error due to such an approximation is then of relative order $\Gamma^{n/2}$, while we need to carry the expansion only to $O(\delta)\gg\Gamma^{n/2}$. Thus to this order we can write $\beta^2=k^2$ throughout.

https://doi.org/10.1017/jfm.2026.11340 Published online by Cambridge University Press

Keeping the two leading-order terms in the coefficients of (2.24) gives

$$b_6 = 16\sigma\left(\tau^2 + 2\gamma\tau\kappa\right)\lambda_2^4\tilde{k}^2\Gamma^{4-n/2}, \tag{3.17a}$$

$$b_4 = \left(-24\sigma\tau^2\tilde{k}^4 - 32\gamma\sigma\tau\kappa\tilde{k}^4 + 4\gamma\left(\sigma + (1+\sigma)\tau^2\right)\tilde{k}^2\right)\lambda_2^3\Gamma^{3-n}, \tag{3.17b}$$

$$\begin{aligned} b_2 = \Big(&12\sigma\tau^2\tilde{k}^6 + 4\sigma\tau(1-\tau)\widetilde{Rs}\tilde{k}^2 + 8\gamma\sigma\tau\kappa\tilde{k}^6 - 8\gamma\sigma\tau\kappa\widetilde{Rs}\tilde{k}^2 \\ &- 2\gamma(\sigma + 2\tau^2(1+\sigma))\tilde{k}^4\Big)\lambda_2^2\Gamma^{2-3n/2}, \end{aligned} \tag{3.17c}$$

$$\begin{aligned} b_0 = \Big(&-2\sigma\tau^2\tilde{k}^8 - 2\sigma\tau(1-\tau)\widetilde{Rs}\tilde{k}^4 \\ &+ \gamma\tau^2(1+\sigma)\tilde{k}^6 + 2\gamma\sigma\tau\kappa\widetilde{Rs}\tilde{k}^4 - \gamma\sigma(1-\tau)\widetilde{Rs}\tilde{k}^2\Big)\lambda_2\Gamma^{1-2n}. \end{aligned} \tag{3.17d}$$

Note that in expressions (3.17), we have not expanded the λ_2 terms into their $O(1)$ and $O(\gamma)$ components. It turns out that there is significant cancellation of the λ_2 terms in (2.23) and we therefore defer to a later stage any λ_2 terms that remain.

It is easily verified that when $\gamma = 0$, equation (2.23) (with coefficients (3.17)) is solved by

$$\omega^2 = \frac{1}{2\lambda_2}\tilde{k}^2\Gamma^{-1-n/2} = \frac{1}{2\lambda_2}k^2\Gamma^{-n/2}. \tag{3.18}$$

To obtain the next order correction to ω^2, we thus write

$$\omega^2 = \frac{1}{2\lambda_2}\left(\tilde{k}^2 + \gamma p\right)\Gamma^{-1-n/2}, \tag{3.19}$$

where we still keep λ_2 unexpanded. From (2.23), at $O(\gamma)$, there is considerable simplification; all of the factors of Γ and λ_2 drop out, with the remaining terms determining p simply as

$$p = \frac{1}{2\tau} + \frac{\tilde{k}^2\kappa}{(1-\tau)}. \tag{3.20}$$

We now use (2.22*b*), correct to $O(\gamma)$, to determine $\widetilde{Ra}$, which we write as $\widetilde{Ra} = \widetilde{Ra}_0 + \gamma\widetilde{Ra}_1$. At this stage we do need to pay heed to the separate $O(1)$ and $O(\gamma)$ terms in λ_2; thus, from (3.16), together with the relation $\lambda_1 + \lambda_2 = 1$, we have

$$\lambda_2^{-1} = (1+\tau) + \gamma\kappa. \tag{3.21}$$

From (2.19*b*,*d*,*f*), together with (3.19)–(3.21), retaining terms up to $O(\gamma)$ and dividing out a common factor of Γ^{-2n}, we obtain

$$a_4\omega^4 = \tau\tilde{k}^8 + \gamma\left(\left(1 + \frac{1+\tau}{2\sigma}\right)\tilde{k}^6 + \kappa\left(\frac{1+\tau}{1-\tau}\right)\tilde{k}^8\right), \tag{3.22a}$$

$$\begin{aligned} a_2\omega^2 = {}& 2\tau\tilde{k}^8 + (1+\tau)\left(\widetilde{Rs} - \widetilde{Ra}_0\right)\tilde{k}^4 \\ &+ \gamma\left(\frac{1}{2}\left(3 + \frac{1+\tau}{\sigma}\right)\tilde{k}^6 + \frac{1+\tau}{2\tau}\left(\widetilde{Rs} - \widetilde{Ra}_0\right)\tilde{k}^2 - (1+\tau)\widetilde{Ra}_1\tilde{k}^4\right) \\ &+ \gamma\kappa\left(\frac{1}{1-\tau}\right)\left((1+\tau)\tilde{k}^8 + 2\left(\widetilde{Rs} - \widetilde{Ra}_0\right)\tilde{k}^4\right), \end{aligned} \tag{3.22b}$$

https://doi.org/10.1017/jfm.2026.11340 Published online by Cambridge University Press

$$a_0 = \tau\tilde{k}^8 + \left(\widetilde{Rs} - \tau\widetilde{Ra}_0\right)\tilde{k}^4 - \gamma\tau\widetilde{Ra}_1\tilde{k}^4. \tag{3.22c}$$

On substituting from expressions (3.22) into (2.22*b*), the $O(1)$ and $O(\gamma)$ terms give

$$\widetilde{Ra}_0 = \tau\widetilde{Rs}, \qquad \widetilde{Ra}_1 = \frac{1}{2}\left(\tilde{k}^2 + \frac{1}{\tau\tilde{k}^2}(1-\tau^2)\widetilde{Rs}\right) + 2\kappa\widetilde{Rs}, \tag{3.23}$$

or, in unscaled variables,

$$Ra^{(o)} = \tau Rs + \gamma\left(\frac{\Gamma^{-n/2}}{2}\left(k^2 + \frac{1}{\tau k^2}(1-\tau^2)Rs\right) + 2\kappa Rs\right). \tag{3.24}$$

Thus $Ra^{(o)}$ is minimised when

$$k_c^4 = \frac{1}{\tau}(1-\tau^2)Rs, \tag{3.25}$$

which is independent of κ at leading order. The excellent agreement between the asymptotic result (3.25) and the full numerical result is shown in figure 5. It should just be noted that in the dip, $Ra_c^{(o)}$ ($=\tau Rs$ at leading order, from (3.23)) and $Ra_c^{(s)}$ ($=Rs/\tau$ at leading order, from (2.21)) are of the same asymptotic order ($O(\Gamma^{-n})$). However, the oscillatory mode is always preferred since $\tau < 1$. Furthermore, $Ra_c^{(o)}$ in the dip ($=\tau Rs$) is also of the same asymptotic order as $Ra_c^{(o)}$ for the classical problem ($=(\sigma+\tau)/(1+\sigma)Rs$ at leading order, from (2.28)). Since $\tau < 1$, it follows that, even in the dip, $Ra_c^{(o)}$ for the M–C problem with $n \geqslant 3$ is lower than that of the classical problem.

Expression (3.25) describes the depth of the dip. Its lateral extent in λ can be estimated by equating the values of $Ra_c^{(o)}$ for the outer solution, given by (3.11), with the value of $Ra_c^{(o)}$ for the inner (dip) solution, which, to leading order, is given by $Ra = \tau Rs$, from (3.23). If we write $\lambda = \lambda_d + \delta$ then, to leading order, (3.11) gives

$$Ra_c^{(o)} = 3\left(\frac{\tau Rs}{2\Gamma\delta(1+\tau)}\right)^{2/3}. \tag{3.26}$$

Equating expression (3.26) with τRs leads to the following estimate of δ, the half-width of the dip:

$$\delta = \frac{3^{3/2}}{2\Gamma(1+\tau)(\tau Rs)^{1/2}}. \tag{3.27}$$

The decrease in the width of the dip with increasing Rs can be clearly seen in figure 5.

3.3.3. *Low wavenumber modes*

The analysis of § 3.3.2 shows that the preferred mode at the dip is a high wavenumber mode, with $k_c^2 = O(\Gamma^{-n/2})$ and $Ra_c^{(o)} = O(\Gamma^{-n})$. For completeness, it is worth noting that there is also a minimum in the $(k^2, Ra^{(o)})$ curve at very low wavenumbers. Guided by the numerical results, the relevant scalings for this low wavenumber mode are $k^2 = O(\Gamma^{n-1})$, $\omega^2 = O(\Gamma^{-1})$, $Ra^{(o)} = O(\Gamma^{-n})$: we may thus write $k^2 = \Gamma^{n-1}\tilde{k}^2$, $\omega^2 = \Gamma^{-1}\tilde{\omega}^2$, $Rs = \Gamma^{-n}\widetilde{Rs}$, $Ra = \Gamma^{-n}\widetilde{Ra}$. With these scalings, the dominant balance in the frequency equation (2.23) is between the $b_2\omega^2$ and b_0 terms, giving, to leading order,

https://doi.org/10.1017/jfm.2026.11340 Published online by Cambridge University Press

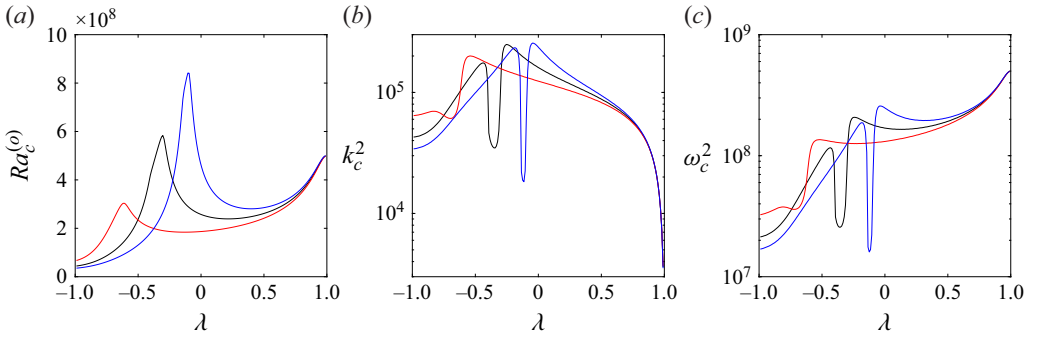


Figure 7. Plots of $Ra_c^{(o)}$, k_c^2 and ω_c^2 versus λ for $\Gamma = 10^{-3}$, $Rs = 10^9$, $\sigma = 1$, with $\tau = 0.2$ (red), $\tau = 0.5$ (black), $\tau = 0.8$ (blue).

$$\tilde{\omega}^2 = \left(\frac{\sigma(1-\tau)}{1+\sigma}\right)\widetilde{Rs}\tilde{k}^2. \tag{3.28}$$

At leading order, (2.22*b*) gives

$$\widetilde{Ra}^{(o)} = \frac{\dfrac{2}{\sigma}\tilde{\omega}^4 - \left(1 + \dfrac{(1+\tau)}{\sigma} + 2\widetilde{Rs}\tilde{k}^2\right)\tilde{\omega}^2 + \widetilde{Rs}\tilde{k}^2}{\tilde{k}^2\left(\tau - 2\tilde{\omega}^2\right)}, \tag{3.29}$$

which simplifies, using (3.28), to

$$\widetilde{Ra}^{(o)} = \left(\frac{\sigma+\tau}{1+\sigma}\right)\widetilde{Rs} \Longrightarrow Ra^{(o)} = \left(\frac{\sigma+\tau}{1+\sigma}\right)Rs. \tag{3.30}$$

The k^2 dependence has dropped out at this order, so to determine k_c^2 we would need to go to higher order. However, this is unnecessary, since the value of $Ra^{(o)}$ for the high wavenumber mode at the dip ($Ra^{(o)} = \tau Rs$ from (3.23)), although of the same order asymptotically as $Ra^{(o)}$ given by (3.30) (i.e. $O(\Gamma^{-n})$), is always lower (recalling that $\tau < 1$). Thus, in the first quadrant the low wavenumber mode is never preferred.

3.3.4. *Varying τ and σ*

In this subsection we consider, numerically, the effects of varying τ and σ. Figure 7 shows $Ra_c^{(o)}$, k_c^2 and ω_c^2 as functions of λ for $n = 3$ with $\sigma = 1$ and for three different values of τ (the $\tau = 0.5$ results are as plotted in figure 4*a–c*). It can be clearly seen that increasing τ leads to the dip in k_c^2 becoming deeper and narrower, in accordance with expressions (3.25) and (3.27). The wider picture, taken across all τ, is provided by the surface plots in figure 8, which show $Ra_c^{(o)}$ and k_c^2 as functions of λ and τ; the dip is the prominent valley in the k_c^2 surface.

In terms of varying σ, the general picture is unchanged between $\sigma = O(1)$ and $\sigma \gg 1$, as illustrated by figure 9, which shows $Ra_c^{(o)}$, k_c^2 and ω_c^2 as functions of λ for $\sigma = 1$, 5, 10. There are strong variations in k_c^2 and ω_c^2 (but not $Ra_c^{(o)}$) near $\lambda = -1$ to adjust to their limiting values at $\lambda = 1$ (see § 4.2.3 of HPE21). For smaller σ, the differences from $\sigma = O(1)$ become more marked. Figure 10 shows $Ra_c^{(o)}$ and k_c^2 as functions of λ and τ for $\sigma = 0.075$ and $\sigma = 0.01$. In comparison with figure 8, it can be seen that decreasing σ

https://doi.org/10.1017/jfm.2026.11340 Published online by Cambridge University Press

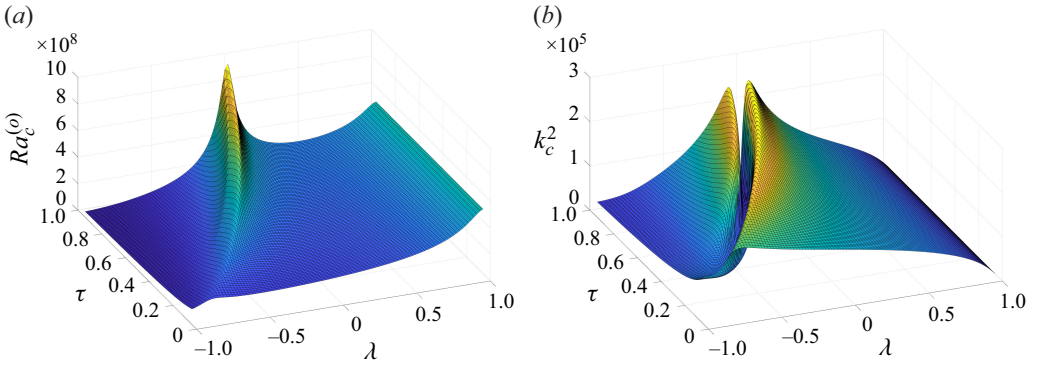


Figure 8. Surface plots of (*a*) $Ra_c^{(o)}$ and (*b*) k_c^2 versus λ and τ for $\Gamma = 10^{-3}$, $Rs = 10^9$, $\sigma = 1$. The range $0.05 \leqslant \tau \leqslant 0.95$ is plotted.

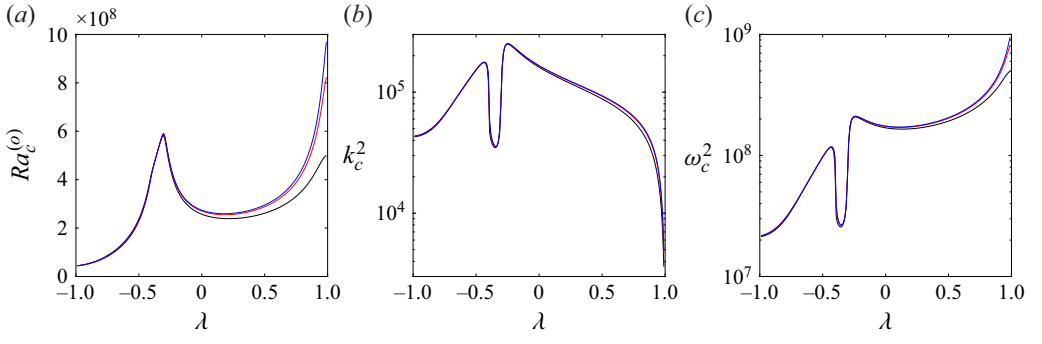


Figure 9. Plots of $Ra_c^{(o)}$, k_c^2 and ω_c^2 versus λ for $\Gamma = 10^{-3}$, $Rs = 10^9$, $\tau = 0.5$, with $\sigma = 1$ (black), $\sigma = 5$ (red), $\sigma = 100$ (blue).

leads to a drastic change in the k_c^2 surface for λ close to -1. The sides of the valley are eroded, first of all to form just an island where higher k_c^2 modes are preferred (figure 10*b*) before the valley disappears altogether (figure 10*d*). The asymptotic analysis of § 3.3.1, performed under the assumption that $\sigma \gtrsim O(1)$, and leading to the results (3.11), is clearly no longer valid. Indeed, one can see that the ordering adopted in § 3.3.1 breaks down once σ is as small as $O(\Gamma^{(n-2)/3})$, i.e. when $\sigma = O(10^{-1})$ for the parameter values of figure 10. Analysing small σ requires a separate asymptotic ordering (or orderings) along the lines pursued by Hughes, Proctor & Eltayeb (2022) in their analysis of the M–C effect in rotating convection: as this would essentially be a further paper in itself, we have restricted our detailed attention here to the case of $\sigma \gtrsim O(1)$.

4. The third quadrant: $Rs < 0$, $Ra < 0$

In the classical double-diffusive problem ($\Gamma = 0$), the onset of instability in the third quadrant is always via a direct instability; the steady mode remains the favoured mode of instability for $n < 2$. However, once $\Gamma^2 Rs$ is of order unity, oscillations can be preferred at onset. These oscillations can arise in a number of ways depending on the value of λ. We first consider the transitional case of $n = 2$. Here there are two different scenarios, described in §§ 4.1 and 4.2. The former occurs in a range of λ including $\lambda = -1$,

https://doi.org/10.1017/jfm.2026.11340 Published online by Cambridge University Press

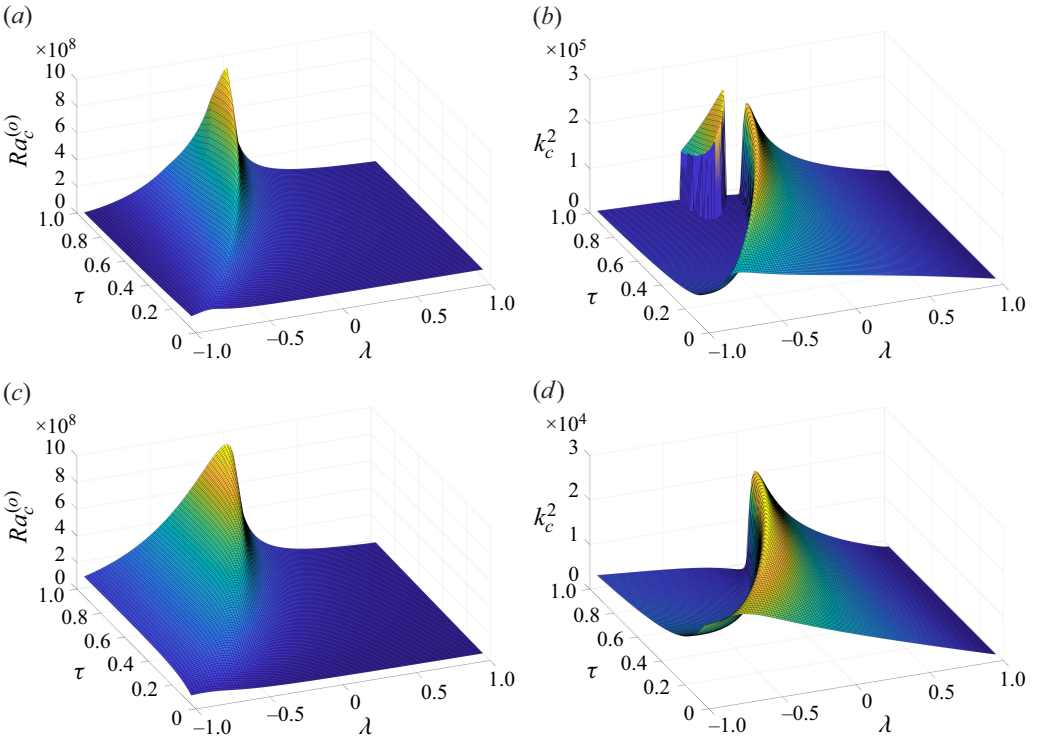


Figure 10. Surface plots of (*a*,*c*) $Ra_c^{(o)}$ and (*b*,*d*) k_c^2 versus λ and τ for $\Gamma = 10^{-3}$, $Rs = 10^9$. In (*a*,*b*), $\sigma = 0.075$; in (*c*,*d*), $\sigma = 0.01$. The range $0.05 \leqslant \tau \leqslant 0.95$ is plotted.

whereas the latter holds for larger values of λ, in a range including $\lambda = 1$. We call these cases 'smaller λ' and 'larger λ', respectively. The global picture for $n = 2$, across all λ, is illustrated in § 4.3. We then consider the situation where $n > 2$, where oscillatory behaviour is generally well established. High wavenumber modes are considered in § 4.4 and low wavenumber modes in § 4.5; these are combined to give the full stability picture in § 4.6.

Since many of the results of the preceding section do not seem to depend on the signs of Ra and Rs, it might be thought that they could be adapted straightforwardly to the analysis of the third quadrant. However, this is not the case. The analogues of minima of Ra in the first quadrant are usually maxima of Ra in the third quadrant, so there is no relation between the preferred wavenumbers in the two cases. In the third quadrant, oscillations appear only if n is sufficiently large, and so the way in which they manifest themselves needs detailed investigation, while in the first quadrant oscillations are possible for all $n > 0$. Finally, the third quadrant counterpart of the remarkable 'dip' phenomenon encountered in the first quadrant differs markedly, as it leads to a region of steady convection rather than a significant change in the oscillation wavenumber.

4.1. $n = 2$: *appearance of oscillations for smaller* λ

We first look for the onset of oscillations in the third quadrant for $n = 2$, when λ is sufficiently negative; in this case, the situation is similar to that described in HPE21 for $\lambda = -1$. Provided σ is sufficiently small, oscillations appear as a loop of marginal solutions, either above or below the steady branch, depending on the parameters.

https://doi.org/10.1017/jfm.2026.11340 Published online by Cambridge University Press

We have performed a series of numerical calculations to establish the dependence of the critical values of Ra, k^2 and ω^2 on Γ. Guided by these results, we deduce that the relevant scalings are Ra, $Rs = O(\Gamma^{-2})$, $k^2 = O(\Gamma^{-1/2})$, $\omega^2 = O(\Gamma^{-2})$: thus we write $Rs = \Gamma^{-2}\widetilde{Rs}$, $Ra = \Gamma^{-2}\widetilde{Ra}$, $k^2 = \Gamma^{-1/2}\tilde{k}^2$, $\omega^2 = \Gamma^{-2}\tilde{\omega}^2$. At leading order, the coefficients of (2.19) then become

$$a_5 = \left(1-\lambda^2\right)\frac{\tilde{k}^2}{\sigma}\Gamma^{3/2}, \tag{4.1a}$$

$$a_4 = \frac{2}{\sigma}\tilde{k}^2\Gamma^{1/2}, \tag{4.1b}$$

$$a_3 = \left(\frac{\tilde{k}^2}{\sigma} + (1-\lambda^2)(\widetilde{Rs}-\widetilde{Ra})\tilde{k}^2\right)\Gamma^{-1/2}, \tag{4.1c}$$

$$a_2 = 2\left(\widetilde{Rs}-\widetilde{Ra}\right)\tilde{k}^2\Gamma^{-3/2}, \tag{4.1d}$$

$$a_1 = \left(\widetilde{Rs}-\widetilde{Ra}\right)\tilde{k}^2\Gamma^{-5/2}, \tag{4.1e}$$

$$a_0 = \left(\widetilde{Rs}-\tau\widetilde{Ra}\right)\tilde{k}^4\Gamma^{-3}. \tag{4.1f}$$

The dominant balance in (2.22*b*) is then between the $a_4\omega^4$ and $a_2\omega^2$ terms, giving, at leading order,

$$\tilde{\omega}^2 - \sigma\left(\widetilde{Rs}-\widetilde{Ra}\right) = 0. \tag{4.2}$$

Turning to the cubic equation for the frequency, (2.23), making the same scaling and keeping only the leading terms, leads to the reduced set of coefficients,

$$b_6 = \sigma\left(1-\lambda^2\right)^2\tilde{k}^2\,\Gamma^{7/2}, \tag{4.3a}$$

$$b_4 = \left(2\sigma(1+\lambda^2)+(1+\lambda)^2\right)\tilde{k}^2\,\Gamma^{3/2}, \tag{4.3b}$$

$$b_2 = \left((1+\sigma)\tilde{k}^2 + \sigma\left((\tau-1)\lambda^2 - 2(1+\tau)\lambda + \tau - 1\right)\widetilde{Rs}\tilde{k}^2\right)\Gamma^{-1/2}, \tag{4.3c}$$

$$b_0 = -\sigma(1-\tau)\widetilde{Rs}\tilde{k}^2\,\Gamma^{-5/2}. \tag{4.3d}$$

Thus, (2.23) can be written at leading order as

$$\sigma\left(1-\lambda^2\right)^2\tilde{\omega}^6 + \left(2\sigma(1+\lambda^2)+(1+\lambda)^2\right)\tilde{\omega}^4 + \left((1+\sigma) - \sigma\left((1-\tau)\lambda^2 + 2(1+\tau)\lambda + 1 - \tau\right)\widetilde{Rs}\right)\tilde{\omega}^2 - \sigma(1-\tau)\widetilde{Rs} = 0. \tag{4.4}$$

In principle, (4.4) can be used to analyse the appearance of loops of marginal oscillations, as in HPE21, although analytical results are in general too elaborate to be useful. We can, however, look for the conditions for which one side of the loop crosses the steady branch, so that $\widetilde{Rs} = \tau\widetilde{Ra}$, or, in view of (4.2),

$$\tilde{\omega}^2 = -\frac{\sigma(1-\tau)\widetilde{Rs}}{\tau}. \tag{4.5}$$

https://doi.org/10.1017/jfm.2026.11340 Published online by Cambridge University Press

On substituting for $\widetilde{Rs}$ from (4.5) into (4.4), we see that a factor of $\tilde{\omega}^2$ may be cancelled, leaving the quadratic for $\tilde{\omega}^2$:

$$\sigma\left(1-\lambda^2\right)^2\tilde{\omega}^4+\left(\left(\lambda^2+1\right)(1+2\sigma+\tau)+2\lambda\frac{1+\tau^2}{1-\tau}\right)\tilde{\omega}^2+(1+\sigma+\tau)=0. \tag{4.6}$$

Equation (4.6) can have real positive solutions for $\tilde{\omega}^2$ only if λ is not too large. In fact, λ must satisfy the following inequality ('$b^2>4ac$'):

$$\lambda^2\left(\sqrt{1+\sigma+\tau}-\sqrt{\sigma}\right)^2+\frac{2\lambda\left(1+\tau^2\right)}{1-\tau}+\left(\sqrt{1+\sigma+\tau}+\sqrt{\sigma}\right)^2<0. \tag{4.7}$$

After a little algebra, we find that this inequality for λ is equivalant to

$$\lambda<\frac{-(1-\tau)}{(\sqrt{1+\sigma+\tau}-\sqrt{\sigma})^2}. \tag{4.8}$$

(The root of larger modulus is less than -1, and thus impermissible.) We have to check that the value of λ given by (4.8) is greater than -1. Replacing the inequality by an equality and λ by -1, we find that

$$\sqrt{\sigma(1+\sigma+\tau)}=\sigma+\tau \quad \text{and, hence, } \sigma=\sigma_c=\frac{\tau^2}{1-\tau}, \tag{4.9}$$

consistent with the results of HPE21. Thus if $\sigma<\sigma_c$ there will be a range of negative λ, and an associated range of $\tilde{\omega}^2$, and hence of $\widetilde{Rs}$, for which the onset of oscillations is coincident with the steady branch when $\widetilde{Ra}=\widetilde{Rs}/\tau$. If $\sigma>\sigma_c$, on the other hand, oscillations are not preferred until $n\gtrsim 3$. The two different scenarios will be discussed further in § 4.3.

In HPE21 we showed that depending on the values of σ and τ, the loop of oscillations appears either above the steady branch, in which case the transition to oscillatory convection occurs when the smaller of the two roots for $|\widetilde{Rs}|$ from (4.5) and (4.6) crosses the line of the steady branch; or below the steady branch, in which case oscillations are preferred just after the point of appearance. The transition between these two regimes occurs on a line $\mathcal{L}$ in (σ,τ) space for each λ; for $\lambda=-1$, this is given by expression (3.29) in HPE21.

For the case of general λ, we can make some progress in finding this line by returning to (4.4), which can be written compactly as

$$A\tilde{\omega}^6+B\tilde{\omega}^4+\left(C-D\widetilde{Rs}\right)\tilde{\omega}^2-E\widetilde{Rs}=0, \tag{4.10}$$

where

$$\begin{aligned} &A=\sigma\left(1-\lambda^2\right)^2,\quad B=2\sigma(1+\lambda^2)+(1+\lambda)^2,\quad C=(1+\sigma),\\ &D=\sigma\left((1-\tau)(1+\lambda^2)+2\lambda(1+\tau)\right),\quad E=\sigma(1-\tau). \end{aligned} \tag{4.11}$$

If (4.10) has a double root, marking the appearance of the loop of oscillations, then we also have

$$3A\tilde{\omega}^4+2B\tilde{\omega}^2+(C-D\widetilde{Rs})=0. \tag{4.12}$$

Combining (4.10) with (4.12) gives a further quadratic in $\tilde{\omega}^2$:

$$B\tilde{\omega}^4+2(C-D\widetilde{Rs})\tilde{\omega}^2-3E\widetilde{Rs}=0. \tag{4.13}$$

We now seek the condition that the loop appears on the steady branch, and hence we can use expression (4.5) in (4.13). On cancelling a factor of $\widetilde{Rs}$, we obtain the following

https://doi.org/10.1017/jfm.2026.11340 Published online by Cambridge University Press

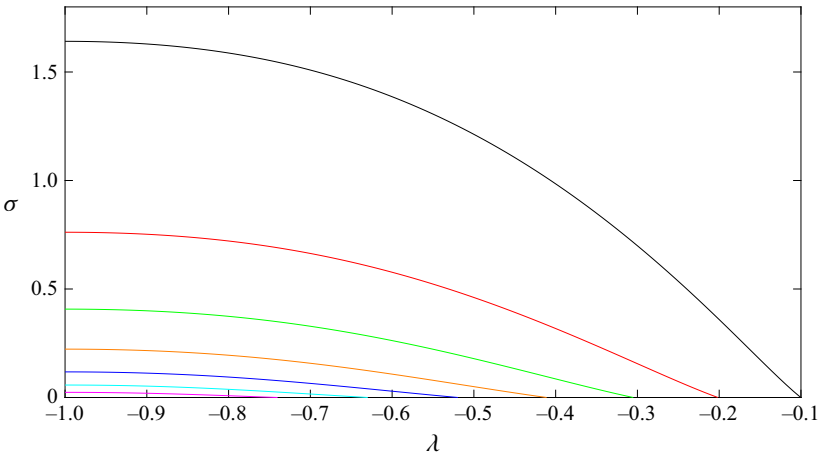


Figure 11. Plot of σ versus λ for the line $\mathcal{L}$, defined by (4.15), denoting the parameter values at which the loop of oscillatory solutions first appears on the steady branch. The curves show $\tau = 0.9$ (top), 0.8, 0.7, 0.6, 0.5, 0.4, 0.3 (bottom).

explicit formula relating the value of $\widetilde{Rs}$ to the other parameters:

$$\widetilde{Rs} = \frac{\tau\,(3\tau + 2(1+\sigma))}{\sigma\left((1+\lambda^2)(1-\tau)(1+2(\tau+\sigma)) + 2\lambda(1+\tau+2\tau^2)\right)} = \frac{F(\sigma,\tau)}{\sigma G(\sigma,\tau,\lambda)} \quad \text{say.} \tag{4.14}$$

Since $\widetilde{Rs} < 0$, this shows that λ cannot be too large and, in particular, must be negative. On substituting for $\tilde{\omega}^2$ and $\widetilde{Rs}$ from (4.5) and (4.14) into (4.12), we obtain the following complicated relation defining the transition line $\mathcal{L}$:

$$3A\sigma(1-\tau)^2F^2 - 2B\sigma\tau(1-\tau)FG + \tau^2G\,(\sigma CG - DF) = 0. \tag{4.15}$$

The line $\mathcal{L}$ is shown for σ as a function of λ for a number of values of τ in figure 11. Each of the curves, which have different fixed values of τ, denotes the value of σ, as a function of λ, for which the loop of oscillatory solutions appears precisely on the steady branch. Above the curve (i.e. at greater values of σ), the loop of oscillatory solutions is born above the steady branch; below the curve (i.e. at smaller σ), the loop of oscillatory solutions is born below the steady branch.

4.2. $n = 2$: *appearance of oscillations for larger* λ

As has been shown above, loops of oscillations cannot appear if λ is too large. For larger values of λ, branches of oscillations can appear via Takens–Bogdanov (T–B) bifurcations from the steady branch. This situation is similar to that described in HPE21 for $\lambda = 1$.

In contrast to the oscillation loops described above, the branches that appear for larger λ have $k^2 \sim \Gamma^{-1}$. The T–B points are characterised by $a_0 = a_1 = 0$ in (2.19). Writing $k^2 = \Gamma^{-1}\tilde{k}^2$, $Rs = \Gamma^{-2}\widetilde{Rs}$, $Ra = \Gamma^{-2}\widetilde{Ra}$, and replacing β^2 by k^2 since $k^2 \gg 1$, we obtain

$$\tau\tilde{k}^4 + \widetilde{Rs} - \tau\widetilde{Ra} = \left(1+\tau+\frac{\tau}{\sigma}\right)\tilde{k}^4 + \widetilde{Rs}\left(1+(1+\lambda)\tilde{k}^2\right) - \widetilde{Ra}\left(1+\tau(1-\lambda)\tilde{k}^2\right) = 0. \tag{4.16}$$

https://doi.org/10.1017/jfm.2026.11340 Published online by Cambridge University Press

Eliminating $\widetilde{Ra}$ between the two equations of (4.16) gives the following cubic for $\tilde{k}^2$:

$$\tau(1-\lambda)\tilde{k}^6 - \tau\left(1+\frac{1}{\sigma}\right)\tilde{k}^4 - 2\lambda\widetilde{Rs}\tilde{k}^2 + \widetilde{Rs}\left(\frac{1}{\tau}-1\right) = 0. \tag{4.17}$$

There are thus either one or three T–B points (noting that $\widetilde{Rs} < 0$ and that we must have $\tilde{k}^2 > 0$). It is instructive to consider the condition under which two T–B points coincide; this results from setting the discriminant of the cubic equation (4.17) to zero, giving

$$32(1-\lambda)\lambda^3 S^2 + \left(4\lambda^2 P^2 - 36\lambda(1-\lambda)PQ - 27(1-\lambda)^2Q^2\right) - 4P^3Q = 0, \tag{4.18}$$

where, to simplify notation, we have introduced $P = 1 + 1/\sigma$, $Q = 1 - 1/\tau$, $S = \widetilde{Rs}/\tau$. The quadratic expression (4.18) for S denotes the two values of S (and hence $\widetilde{Rs}$) between which there are three T–B points. By seeking the condition for these two values of Rs to be repeated, we may then identify the critical values of λ at which the possibility of three T–B points disappears. Setting the discriminant of the quadratic (4.18) to zero gives

$$\left(4\lambda^2 P^2 - 36\lambda(1-\lambda)PQ - 27(1-\lambda)^2Q^2\right)^2 + 512\lambda^3(1-\lambda)P^3Q = 0. \tag{4.19}$$

On making the further substitutions

$$C = \lambda P, \qquad D = (1-\lambda)Q, \qquad C = \Delta D, \quad \text{where} \quad \Delta = -\frac{\lambda(1+\sigma)\tau}{(1-\lambda)\sigma(1-\tau)}, \tag{4.20}$$

we obtain a (quartic) expression involving only Δ, which, rather remarkably, factorises as

$$0 = (4\Delta^2 - 36\Delta - 27)^2 + 512\Delta^3 = 16(\Delta + 9/2)^3(\Delta + 1/2). \tag{4.21}$$

On rearranging the expression for Δ in (4.20), the two distinct roots of (4.21) thus give the following values of λ for which there are coincident T–B points:

$$\lambda_a = \frac{9\sigma(1-\tau)}{9\sigma + 2\tau - 7\sigma\tau} \qquad \text{and} \qquad \lambda_b = \frac{\sigma(1-\tau)}{\sigma + 2\tau + \sigma\tau}. \tag{4.22}$$

Recall that here we are interested in the third quadrant and so $Rs < 0$; this in turn requires (recalling $Q < 0$) that the coefficient of S in (4.18) is positive. We find that only for $\lambda = \lambda_a$ ($\Delta = -9/2$) is this satisfied. Thus, we have the possibility of three T–B points (depending on the value of $\widetilde{Rs}$) for $1 > \lambda > \lambda_a$ and one T–B point otherwise. (The value λ_b denotes such a transition point in the first quadrant. However, oscillatory modes are favoured there, with the steady mode out of contention, as discussed in § 3; T–B points thus play no role in determining the overall stability boundary in the first quadrant.)

The role of the T–B points can be seen through numerical calculation of the steady and oscillatory boundaries for $\lambda < \lambda_a$ and $\lambda > \lambda_a$. For illustration, we consider the case of $\sigma = 0.2$, $\tau = 0.5$, for which $\lambda_a = 3/7 \approx 0.429$. Figure 12 shows the stability boundaries for $\lambda = 0.3$, for which there can only be one T–B point. In figure 12(*a*), $\widetilde{Rs} = -10$; the oscillatory branch emerging from the T–B point always lies above the minimum of the steady branch (given by $Ra_c^{(s)} = Rs/\tau$), and thus, steady convection is favoured. In figure 12(*b*), $\widetilde{Rs} = -31.48$, the value at which the critical Rayleigh numbers for the (low wavenumber) steady and (high wavenumber) oscillatory modes are identical. In figure 12(*c*), $\widetilde{Rs} = -40$; although the T–B point itself lies above $Ra = Ra_c^{(s)}$, the oscillatory branch emerging from the T–B points dips down sufficiently that high wavenumber oscillatory modes are favoured.

https://doi.org/10.1017/jfm.2026.11340 Published online by Cambridge University Press

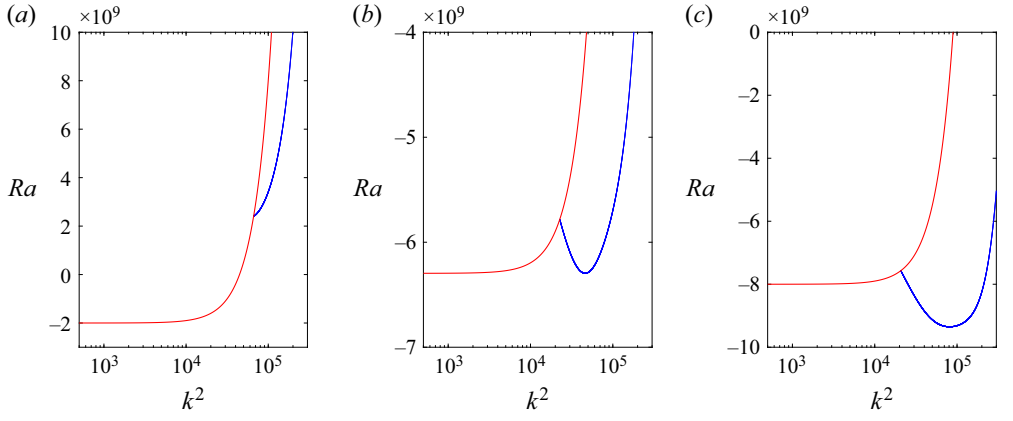


Figure 12. Plots of Ra versus k^2 for the steady (red) and oscillatory (blue) stability boundaries, with $\Gamma = 10^{-4}$, $\sigma = 0.2$, $\tau = 0.5$, $\lambda = 0.3$. In (a), $Rs = -10^9$ ($\widetilde{Rs} = -10$); in (b), $Rs = -3.148 \times 10^9$ ($\widetilde{Rs} = -31.48$); in (c), $Rs = -4 \times 10^9$ ($\widetilde{Rs} = -40$).

For $\lambda > \lambda_a$, where there is always a range of $\widetilde{Rs}$ for which there are three T–B points, we have identified two ways in which the oscillatory branches can evolve, dependent on the proximity of λ to λ_a. Figure 13$(a$–$c)$ shows the stability boundaries for $\lambda = 0.5$, i.e. for λ slightly greater than λ_a. There are three T–B points in the range $-10.945 < \widetilde{Rs} < -9.868$. Figure 13$(a)$ shows the loop of oscillatory solutions created at $\widetilde{Rs} = -9.868$, together with the branch of oscillatory solutions emerging from the higher T–B point. Note that steady solutions are preferred. At $\widetilde{Rs} = -10.945$, shown in figure 13(b), the two oscillatory branches have merged, via coalescence of the upper two T–B points; again, steady solutions are still preferred. For $\widetilde{Rs} < -10.945$, there is only one oscillatory branch; for sufficiently negative values of $\widetilde{Rs}$, oscillatory solutions become preferred, as shown in figure 13(c).

Figure 13$(d$–$f)$ shows the stability boundaries for $\lambda = 0.8$, i.e. for λ now rather greater than λ_a. There are three T–B points in the range $-14.681 < \widetilde{Rs} < -4.490$. We can see from figure 13(d) that the loop of oscillatory solutions created at $\widetilde{Rs} = -4.490$ and the branch of oscillatory solutions emerging from the higher T–B point have both developed a pronounced 'hook'. Furthermore, by this value of $\widetilde{Rs}$, oscillatory modes have already become preferred. As $\widetilde{Rs}$ is made more negative, the oscillatory branches meet when $\widetilde{Rs} = -10.466$, as shown in figure 13(e); in contrast to the case illustrated in figure 13$(a$–$c)$, the oscillatory branches merge before coalescence of the upper two T–B points. The oscillatory branches reconnect, as shown in figure 13(f) for $\widetilde{Rs} = -12$. The upper two T–B points merge and disappear at $\widetilde{Rs} = -14.681$.

4.3. *Transition between steady and oscillatory onset for general λ*

The foregoing results have shown that, for sufficiently large (negative) values of Rs, oscillatory convection can be preferred. The occurrence of oscillations in this quadrant is due entirely to the M–C effect, since in the classical case only steady-state bifurcations are possible. When $\sigma < \sigma_c = \tau^2/(1-\tau)$ (see (4.9)), the transition to oscillatory behaviour occurs for $|Rs| = O(\Gamma^{-n})$, where Γ is generally between 2 and 3, while when $\sigma > \sigma_c$, oscillatory behaviour is preferred only at values of $n \gtrsim 3$ for smaller λ. The critical wavenumber of the oscillatory mode at the transition between steady and oscillatory modes is also much larger when $\sigma > \sigma_c$.

https://doi.org/10.1017/jfm.2026.11340 Published online by Cambridge University Press

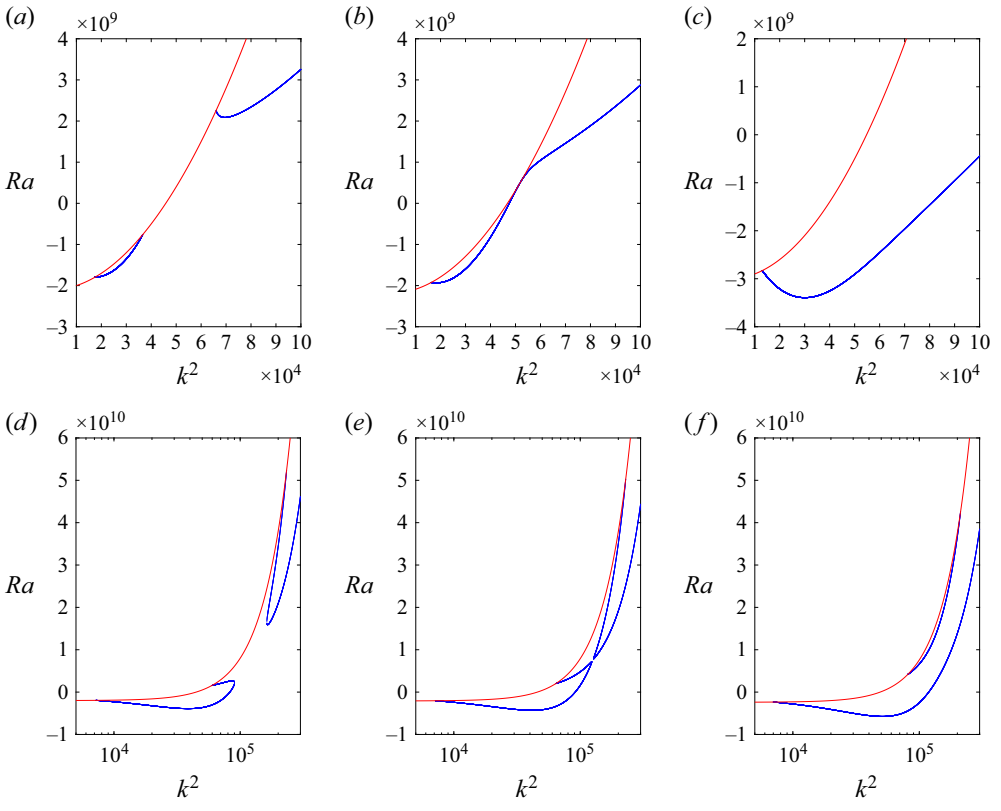


Figure 13. Plots of Ra versus k^2 for the steady (red) and oscillatory (blue) stability boundaries, with $\Gamma = 10^{-4}$, $\sigma = 0.2$, $\tau = 0.5$. In (*a–c*), $\lambda = 0.5$; in (*d–f*), $\lambda = 0.8$. In (*a*), $\widetilde{Rs} = -10.5$ ($Rs = -1.05 \times 10^9$); in (*b*), $\widetilde{Rs} = -10.945$ ($Rs = -1.0945 \times 10^9$); in (*c*), $\widetilde{Rs} = -15$ ($Rs = -1.5 \times 10^9$); in (*d*), $\widetilde{Rs} = -10$ ($Rs = -10^9$); in (*e*), $\widetilde{Rs} = -10.466$ ($Rs = -1.0466 \times 10^9$); in (*f*), $\widetilde{Rs} = -12$ ($Rs = -1.2 \times 10^9$).

Figure 14 gives a global picture of the dependence of the transition values on λ for two cases: (i) $\tau = 0.5$, $\sigma = 0.2$ ($\sigma < \sigma_c$); (ii) $\tau = 0.5$, $\sigma = 1$ ($\sigma > \sigma_c$). In this figure the value of $|Rs|$ is represented by n with $Rs = -\Gamma^{-n}$. The curves are constructed using an iterative process by which the critical values k_c^2 and $Ra_c^{(o)}$ are calculated for a given n and then n is adjusted until $Ra^{(o)} = Ra^{(s)}$ at $n = n_c$, $k_c^2 = k_{oc}^2$. The figure thus incorporates the results of both §§ 4.1 and 4.2. It can be seen that in both cases the critical value n_c climbs sharply as λ approaches the 'dip' value of $\lambda_d = (\tau - 1)/(\tau + 1)$; $\lambda \approx \lambda_d$ is where anomalous behaviour of the critical wavenumber appears in the first quadrant. As we shall show in § 4.5, for $\lambda \approx \lambda_d$ in the third quadrant, steady onset is always preferred, so that there is in fact no dip in the critical oscillatory wavenumber in the third quadrant case.

4.4. $n \geqslant 3$: *high wavenumber*

When $n > 2$, and in particular when $n \gtrsim 3$, oscillations are usually favoured except for particular values of the parameters. The favoured mode of oscillation can occur either at large or small wavenumber. In this subsection we investigate the high wavenumber modes; the low wavenumber modes will be discussed in § 4.5. In this high wavenumber regime,

https://doi.org/10.1017/jfm.2026.11340 Published online by Cambridge University Press

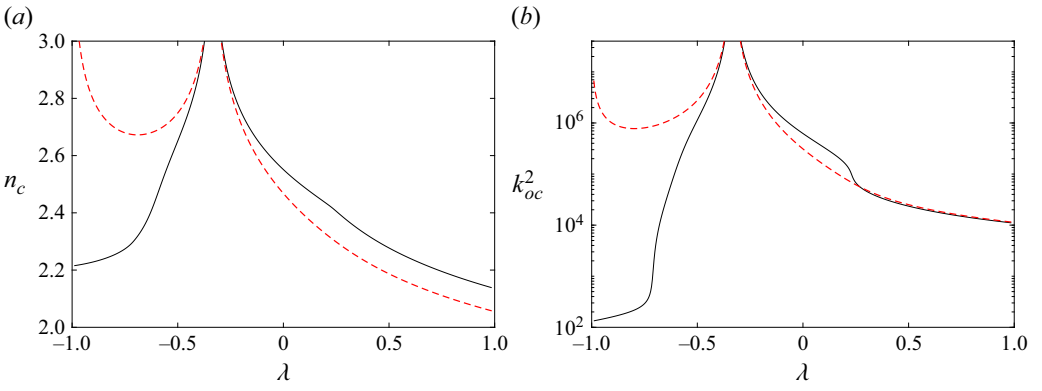


Figure 14. Plots of (*a*) n_c and (*b*) k_{oc}^2 versus λ for $\Gamma = 10^{-4}$, $\tau = 0.5$. The black lines denote $\sigma = 0.2$ ($\sigma < \sigma_c$), the red dashed lines $\sigma = 1$ ($\sigma > \sigma_c$).

numerical results suggest the scaling $k^2 \sim \Gamma^{1-n}$; we thus write $k^2 = \Gamma^{1-n}\tilde{k}^2$ and take $\beta^2 = k^2$ at leading order.

The frequency is then determined from (2.24); with the above scaling for k^2, and assuming that we are not particularly close to $\lambda = \pm 1$, so that $1 - \lambda^2$ is not small, we find that the coefficients of (2.24) have $b_6 \sim \Gamma^{5-n}$, $b_4 \sim \Gamma^{5-2n}$, $b_2 \sim \Gamma^{5-3n}$, $b_0 \sim \Gamma^{5-4n}$. Thus, on rescaling $\omega^2 = \tilde{\omega}^2\Gamma^{-n}$, and cancelling a common factor of σ, we obtain the leading-order cubic equation for $\tilde{\omega}^2$:

$$\left(1-\lambda^2\right)^2\tilde{k}^2\tilde{\omega}^6 - \left(1-\lambda^2\right)\left(1+2\tau+\lambda(1-2\tau)\right)\tilde{k}^4\tilde{\omega}^4 + \tau\left((\tau-2)\lambda^2 - 2\tau\lambda + 2 + \tau\right)\tilde{k}^6\tilde{\omega}^2 - (1-\lambda)\tau^2\tilde{k}^8 = 0. \tag{4.23}$$

Note that the critical frequency does not depend on σ at leading order. On introducing λ_1, λ_2 as in (2.13) and writing $X = \tilde{\omega}^2/\tilde{k}^2$, (4.23) simplifies to

$$(2\lambda_2 X - 1)(2\lambda_1 X - \tau)^2 = 0, \quad \text{so that} \quad X = \frac{1}{2\lambda_2}, \quad X = \frac{\tau}{2\lambda_1} \ \text{(repeated)}. \tag{4.24}$$

We now seek to determine Ra by using the coefficients $a_1, \ldots, a_5$ defined in (2.12), and considering (2.22*b*), namely $a_4\omega^4 - a_2\omega^2 + a_0 = 0$. To bring Ra into play at leading order suggests *a priori* that $Ra \sim k^4 \sim \Gamma^{2-2n}$. However, for both values of X in (4.24), we find that $Ra = 0$ in this scaling. This conclusion is supported by the numerical results. For example, with $n = 4$ and $\Gamma = 10^{-4}$, $Ra \sim \Gamma^{2-2n}$ would give $Ra = O(10^{24})$, whereas the computed value of Ra_c is actually $O(10^{18})$.

We are thus led to the revised scalings $k_c^2 \sim \Gamma^{1-n}$, $\omega_c^2 \sim \Gamma^{-n}$, $Ra_c \sim \Gamma^{1-3n/2}$, where the presence of $n/2$ in the exponent of Γ for Ra_c derives from a half-power correction to X, which, in turn, follows from the double root in (4.24). The value of Ra corresponding to the non-repeating root is much smaller in magnitude ($O(\Gamma^{-n})$), and hence we do not need to consider this root further. The corrections to b_4, b_2 and b_0 have relative magnitude Γ^{n-2}, which we denote by ε. Returning to using $\tilde{\omega}^2$ and $\tilde{k}^2$, and now keeping the zeroth- and first-order terms, we may express (2.23) in the form

$$b_{60}\tilde{\omega}^6 + (b_{40} + \varepsilon b_{41})\tilde{\omega}^4 + (b_{20} + \varepsilon b_{21})\tilde{\omega}^2 + b_{00} + \varepsilon b_{01} = 0, \tag{4.25}$$

https://doi.org/10.1017/jfm.2026.11340 Published online by Cambridge University Press

where

$$b_{60} = \sigma\left(1-\lambda^2\right)^2, \tag{4.26a}$$

$$b_{40} = -\sigma(1-\lambda^2)\left(1+2\tau+\lambda(1-2\tau)\right)\tilde{k}^2, \tag{4.26b}$$

$$b_{41} = 2\sigma(1+\lambda^2)+(1+\lambda)^2, \tag{4.26c}$$

$$b_{20} = \sigma\tau\left((\tau-2)\lambda^2-2\tau\lambda+2+\tau\right)\tilde{k}^4, \tag{4.26d}$$

$$b_{21} = -\left(\sigma+2\tau(1+\sigma)+\lambda\left(2\tau(1+\sigma)-\sigma\right)\right)\tilde{k}^2 + \sigma\left((\tau-1)\lambda^2-2(\tau+1)\lambda+\tau-1\right)\widetilde{Rs}, \tag{4.26e}$$

$$b_{00} = -(1-\lambda)\sigma\tau^2\tilde{k}^6, \tag{4.26f}$$

$$b_{01} = \tau^2(1+\sigma)\tilde{k}^4+2\sigma\tau\lambda\widetilde{Rs}\tilde{k}^2. \tag{4.26g}$$

The correction to the repeated root is $O(\varepsilon^{1/2})$; thus we write

$$\tilde{\omega}^2 = \frac{\tau\tilde{k}^2}{(1+\lambda)}+\varepsilon^{1/2}\tilde{\omega}_1^2 = \tilde{\omega}_0^2+\varepsilon^{1/2}\tilde{\omega}_1^2. \tag{4.27}$$

The $O(\varepsilon)$ terms in (4.25) give

$$\sigma(1-\lambda)\left((1+\lambda)\tilde{\omega}_1^2\right)^2\left((1-\lambda)\tilde{\omega}_0^2-\tilde{k}^2\right) = -b_{41}\tilde{\omega}_0^4-b_{21}\tilde{\omega}_0^2-b_{01}, \tag{4.28}$$

which, after some algebra, leads to

$$\tilde{\omega}_1^4 = -\frac{\tau}{(1+\lambda)^3}\left(\tilde{k}^2+(1+\lambda)\widetilde{Rs}\right) = \frac{\tau}{(1+\lambda)^3}\left((1+\lambda)|\widetilde{Rs}|-\tilde{k}^2\right), \tag{4.29}$$

since $Rs<0$. This expression is, remarkably, also independent of σ.

Using (2.22*b*), we can now determine the critical value of Ra. We know that at leading order, Ra does not appear. Then we may write, symbolically,

$$\tilde{a}_4 = \tilde{a}_{40}+O(\varepsilon), \quad \tilde{a}_2 = \tilde{a}_{20}+\varepsilon^{1/2}\tilde{a}_{21}+O(\varepsilon), \quad \tilde{a}_0 = \tilde{a}_{00}+\varepsilon^{1/2}\tilde{a}_{01}+O(\varepsilon), \tag{4.30}$$

where the $\tilde{a}_{21}$ and $\tilde{a}_{01}$ terms are those containing Ra. After some algebra, the $O(\varepsilon^{1/2})$ terms in (2.22*b*) give

$$\tilde{k}^4\left((1-\lambda)\tilde{\omega}_0^2-\tilde{k}^2\right)(1+\lambda)\tilde{\omega}_1^2 = 2\widetilde{Ra}\tilde{k}^2\tilde{\omega}_0^2-\tau\widetilde{Ra}\tilde{k}^4. \tag{4.31}$$

On substituting for $\tilde{\omega}_0^2$ and $\tilde{\omega}_1^2$ from (4.27) and (4.29), and rearranging, (4.31) gives

$$\widetilde{Ra} = \widetilde{Ra}^{(o)} = -\frac{|(1-\lambda)\tau-(1+\lambda)|}{(1-\lambda)\left(\tau(1+\lambda)\right)^{1/2}}\left((1+\lambda)|\widetilde{Rs}|\tilde{k}^4-\tilde{k}^6\right)^{1/2}. \tag{4.32}$$

We note from (4.29) that there are positive and negative roots for $\tilde{\omega}_1^2$; in (4.32) we have chosen the appropriate solution for $\tilde{\omega}_1^2$, dependent on whether $\lambda<\lambda_d$ or $\lambda>\lambda_d$, to make $\widetilde{Ra}^{(o)}<0$, as required. From (4.32), $\widetilde{Ra}^{(o)}$ is minimised when

$$\tilde{k}^2 = \tilde{k}_c^2 = \frac{2(1+\lambda)|\widetilde{Rs}|}{3} \Longrightarrow k_c^2 = \frac{2\Gamma(1+\lambda)|Rs|}{3}, \tag{4.33}$$

https://doi.org/10.1017/jfm.2026.11340 Published online by Cambridge University Press

giving

$$\widetilde{Ra}_c^{(o)} = -\frac{2}{3^{3/2}}\left(\frac{1+\lambda}{1-\lambda}\right)\left(\frac{|(1-\lambda)\tau-(1+\lambda)|}{\tau^{1/2}}\right)|\widetilde{Rs}|^{3/2} \tag{4.34}$$

or, equivalently,

$$Ra_c^{(o)} = -\frac{2\Gamma}{3^{3/2}}\left(\frac{1+\lambda}{1-\lambda}\right)\left(\frac{|(1-\lambda)\tau-(1+\lambda)|}{\tau^{1/2}}\right)|Rs|^{3/2}. \tag{4.35}$$

In the scaling of this subsection, $Ra_c^{(o)}$ vanishes (and so has a maximum) when $\lambda = \lambda_d$, the critical dip value in the first quadrant. In § 4.5 we discuss whether a similar dip appears in the third quadrant.

We note also that expression (4.35) does not hold for $\lambda = \pm 1$ and so different scalings must apply near these endpoints. The connections between the results of this subsection and the endpoint results from HPE21 are discussed below in § 4.6.

4.5. $n \geqslant 3$: *low wavenumber*

In both the first and third quadrants, there is a minimum in $Ra^{(o)}$ at very small k^2. In general, this minimum is at a different asymptotic level to $Ra_c^{(o)}$ at high k^2 and is not of interest. However, at the dip, it can be of the same order, and so we need to establish whether low wavenumber oscillations can be preferred (for the first quadrant low wavenumber modes, we showed in § 3.3.3 that this was never the case).

Guided by numerical results, we adopt the following scalings for k^2, ω^2 and Rs:

$$k^2 = \Gamma^{n-2}\tilde{k}^2, \quad \omega^2 = \Gamma^{-2}\tilde{\omega}^2, \quad Rs = \Gamma^{-n}\widetilde{Rs}. \tag{4.36}$$

From the frequency equation (2.23), $\tilde{\omega}^2$ obeys the following leading-order equation:

$$\sigma\left(1-\lambda^2\right)^2\tilde{\omega}^6 + \left(2\sigma(1+\lambda^2)+(1+\lambda)^2\right)\tilde{\omega}^4 + \left((1+\sigma)+\sigma\left((\tau-1)\lambda^2-2(\tau+1)\lambda+\tau-1\right)\widetilde{Rs}\tilde{k}^2\right)\tilde{\omega}^2 - \sigma(1-\tau)\widetilde{Rs}\tilde{k}^2 = 0. \tag{4.37}$$

In (2.22*b*) the dominant balance is between the first two terms, giving

$$\widetilde{Ra} = \widetilde{Rs} - \frac{\tilde{\omega}^2}{\sigma\tilde{k}^2}. \tag{4.38}$$

Expression (4.37) determines $\tilde{\omega}^2$ (and hence $\widetilde{Ra}^{(o)}$ from (4.38)) as a function of $\tilde{k}^2$. For the critical value $Ra_c^{(o)}$, where $\mathrm{d}\widetilde{Ra}/\mathrm{d}\tilde{k}^2 = 0$, (4.38) implies that

$$\frac{\mathrm{d}\tilde{\omega}^2}{\mathrm{d}\tilde{k}^2} = \frac{\tilde{\omega}^2}{\tilde{k}^2}. \tag{4.39}$$

Expressions (4.37)–(4.39) may be combined to eliminate $\tilde{\omega}^2$, yielding a quadratic equation for k_c^2, with one admissible root. However, this does not lead to a simple formula for the critical value of Ra. That being said, we can nonetheless make progress in addressing the key point of whether the oscillatory branch can ever reach the steady branch in the dip region (which would then suggest that oscillations can be preferred for some parameter values).

https://doi.org/10.1017/jfm.2026.11340 Published online by Cambridge University Press

Substituting the critical value for the onset of steady convection ($\widetilde{Ra} = \widetilde{Rs}/\tau$) into (4.38) gives

$$\widetilde{Rs} = \frac{\tau}{\sigma(\tau - 1)} \frac{\tilde{\omega}^2}{\tilde{k}^2}. \tag{4.40}$$

On substituting for $\widetilde{Rs}$ from (4.40) and for the dip value of $\lambda = (\tau - 1)/(\tau + 1)$ into (4.37), and simplifying, we then obtain the following quadratic for $\tilde{\omega}^2$:

$$16\tau^2\tilde{\omega}^4 + 4\sigma(1 + \tau^2)(1 + \tau)^2\tilde{\omega}^2 + (1 + \sigma + \tau)(1 + \tau)^4 = 0. \tag{4.41}$$

In principle, expression (4.41) gives the frequency of the oscillatory mode at the point where the oscillatory branch crosses the steady branch (at the dip parameter values). However, we can see that there are no real positive solutions for $\tilde{\omega}^2$. Hence, the oscillatory branch never reaches the steady branch and so steady modes are always preferred to low wavenumber oscillations in the dip region. Furthermore, numerical solutions and the results of § 4.4 demonstrate that at the dip values, high wavenumber oscillations can occur only at much smaller (negative) values of Ra than for steady convection. Thus, at the dip, the high wavenumber (oscillatory) mode gives way to the steady branch.

4.6. $n \geqslant 3$: *combined results across all wavenumbers*

We have seen from the results above that when $n \gtrsim 3$, the preferred mode of convection is oscillatory over a wide range of values of λ. Away from the dip value λ_d and the endpoints $\lambda = \pm 1$, the dominant mode has a high critical wavenumber; as λ approaches λ_d, the critical value of Ra for oscillations increases, and for fixed λ near the dip is $O(\Gamma^{1-3n/2})$. As $|\lambda - \lambda_d|$ becomes small, $O(\Gamma^{n/2-1})$, the (negative) value of Ra increases towards zero and the preferred mode of instability is steady convection, with a critical wavenumber of order unity and $|Ra| = O(\Gamma^{-n})$. There is also, in principle, an oscillatory convection mode at low wavenumber, which near the dip can exhibit a critical value comparable with that of classical steady convection, but this mode is never preferred.

The results for general λ away from λ_d cease to hold when λ is close to 1 or -1. Indeed, from the results of HPE21, when $\lambda = \pm 1$, Ra_c (and also k_c^2 and ω_c^2) exhibits a different asymptotic ordering to that displayed in (4.35). At $\lambda = -1$, the onset of instability is steady if $\sigma > \sigma_c = \tau^2/(1 - \tau)$, with

$$Ra_c^{(s)} \approx \frac{Rs}{\tau}, \tag{4.42}$$

and oscillatory if $\sigma < \sigma_c$, with

$$Ra_c^{(o)} \approx \frac{(\sigma + \tau)Rs}{\sigma}. \tag{4.43}$$

At $\lambda = 1$, the onset of instability is always oscillatory, with

$$Ra_c^{(o)} \approx -\Gamma^2 Rs^2. \tag{4.44}$$

The transition between the result (4.35), valid for general λ apart from $\lambda = \pm 1$ and at the dip, and the endpoint results (4.42)–(4.44) is achieved through boundary layers close to $\lambda = \pm 1$. As in § 3.3.1, we may estimate the width of the boundary layers by supposing that the endpoint solutions vary slowly with λ, and then finding the value of λ for which the interior value of Ra_c, given by (4.35), matches the appropriate endpoint value. Thus, the

https://doi.org/10.1017/jfm.2026.11340 Published online by Cambridge University Press

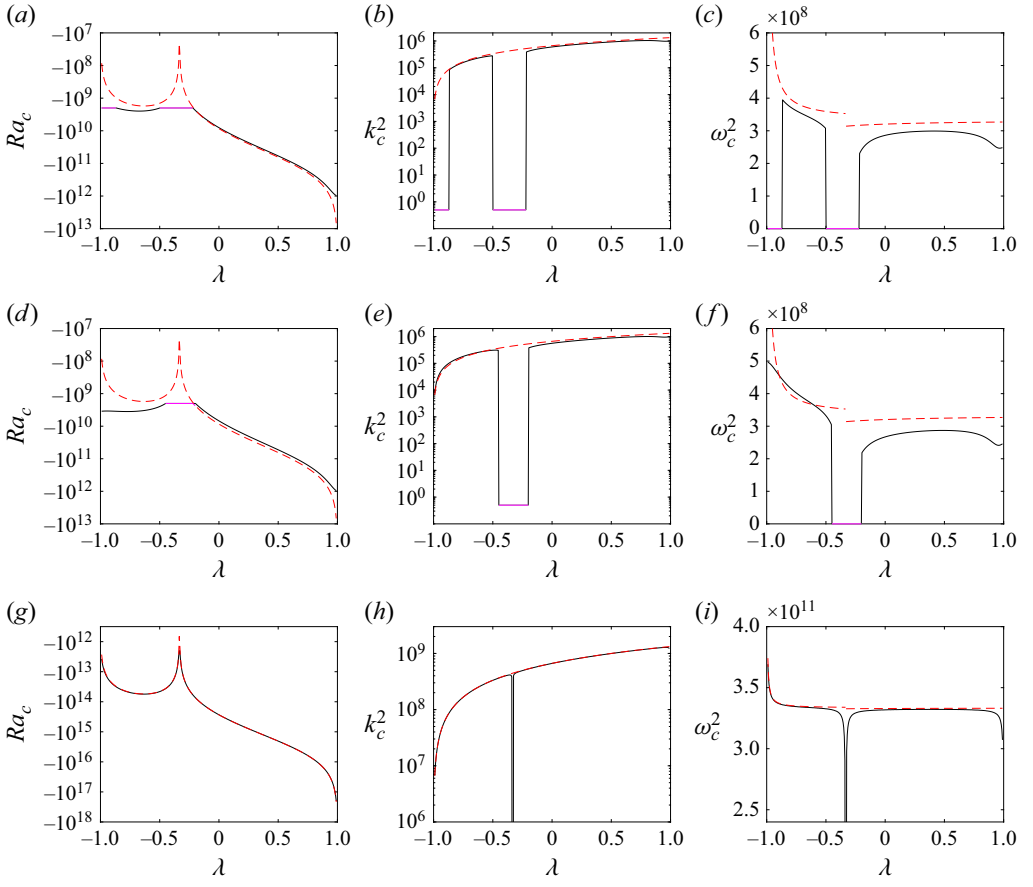


Figure 15. Plots of Ra_c, k_c^2 and ω_c^2 versus λ; $\tau = 0.5$. In (*a–c*), $\sigma = 1$, $\Gamma = 10^{-3}$, $Rs = -10^9$ ($n = 3$); in (*d–f*), $\sigma = 0.2$, $\Gamma = 10^{-3}$, $Rs = -10^9$ ($n = 3$); in (*g–i*), $\sigma = 1$, $\Gamma = 10^{-3}$, $Rs = -10^{12}$ ($n = 4$). Numerical results are shown as solid lines; black (magenta) denotes oscillatory (steady) solutions. The asymptotic results of § 4.4 are shown as dashed red lines.

boundary layer close to $\lambda = -1$ ($\lambda_1 = 0$) has width

$$\delta\lambda_1 = O\left((\Gamma^2|Rs|\tau^3)^{-1/2}\right) \ (\sigma > \sigma_c); \quad \delta\lambda_1 = O\left((\sigma+\tau)(\sigma^2\Gamma^2|Rs|\tau)^{-1/2}\right) \ (\sigma < \sigma_c). \tag{4.45}$$

Finally, the boundary layer close to $\lambda = 1$ has width

$$\delta\lambda_2 = O\left((\Gamma^2|Rs|\tau)^{-1/2}\right). \tag{4.46}$$

Figure 15 gives an overview of the behaviour of the critical values of Ra, k^2 and ω^2, calculated numerically, as functions of λ in the third quadrant. The respective asymptotic results (4.35), (4.33) and (4.27) (combined with (4.29)) are also shown. The dip, in which the critical wavenumber is dramatically reduced and the preferred mode becomes steady for a range of λ, can be clearly seen. In figure 15(*a–c*), $n = 3$ and $\sigma = 1 > \sigma_c = 0.5$; close to $\lambda = -1$, the onset of instability is thus steady. In figure 15(*d–f*), $n = 3$ and $\sigma = 0.2 < \sigma_c$; the onset of instability therefore remains oscillatory up to $\lambda = -1$. Figure 15(*g–i*) is as for figure 15(*a–c*), but with $n = 4$. In comparison with the $n = 3$ plots, two features

https://doi.org/10.1017/jfm.2026.11340 Published online by Cambridge University Press

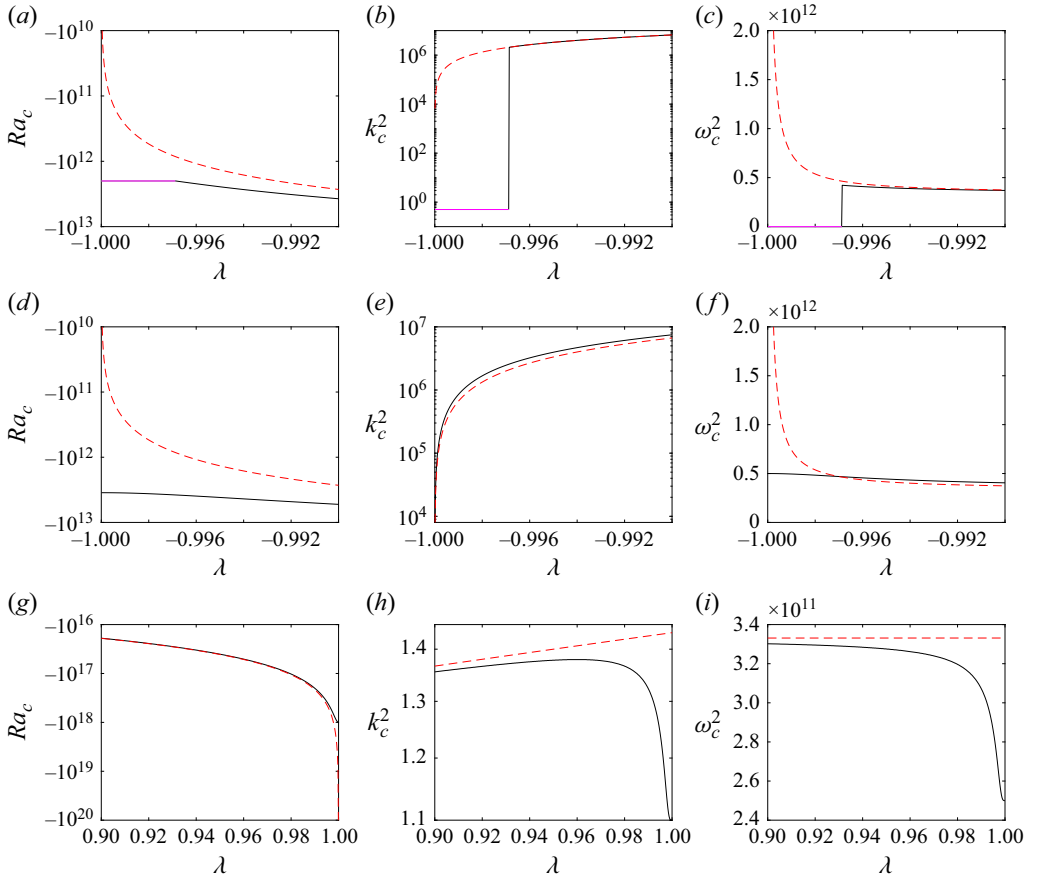


Figure 16. Plots of Ra_c, k_c^2 and ω_c^2 versus λ; $\tau = 0.5$, $\Gamma = 10^{-3}$, $Rs = -10^{12}$ ($n = 4$). (*a–c*) Region near $\lambda = -1$ for $\sigma = 1$; (*d–f*) region near $\lambda = -1$ for $\sigma = 0.2$; (*g–i*) region near $\lambda = 1$ for $\sigma = 1$. Numerical results are shown as solid lines; black (magenta) denotes oscillatory (steady) solutions. The asymptotic results of § 4.4 are shown as dashed red lines.

are apparent: the width of the dip is markedly reduced and the agreement between the numerical and asymptotic results is dramatically improved.

Figure 16 shows the behaviour of the critical values of Ra, k^2 and ω^2 for $n = 4$ close to $\lambda = -1$ and $\lambda = 1$, highlighting the thin transition regions between the solutions at the endpoint and in the interior. In figure 16(*a–c*), $\sigma > \sigma_c$ and there is a transition to steady onset in a region of width $\delta\lambda_1$ given by (4.45) (this thin transition region is too narrow to be seen in figure 15*g–i*). In figure 16(*d–f*), $\sigma < \sigma_c$; onset remains oscillatory up to $\lambda = -1$, but there is again a transition between the interior and endpoint solutions, now in a region of width $\delta\lambda_1$ again given by (4.45). Figure 16(*g–i*) shows the transition between interior and endpoint solutions over a region of width $\delta\lambda_2$ given by (4.46).

The surface plots of figure 17 show Ra_c and k_c^2 as functions of λ and τ for $\sigma = 1$ and $n = 3$. The k_c^2 surface shows clearly the two disconnected regions of oscillatory solutions at high values of k^2, separated by a flat valley of steady solutions, with $k_c^2 = 0.5$. For small τ, the Ra_c surface extending from $\lambda = -1$ is flat (independent of λ) before turning downhill as the oscillatory solution is preferred. For larger values of τ, there is a 'bowl' where high wavenumber oscillatory solutions are preferred; at such values of τ, with increasing λ the

https://doi.org/10.1017/jfm.2026.11340 Published online by Cambridge University Press

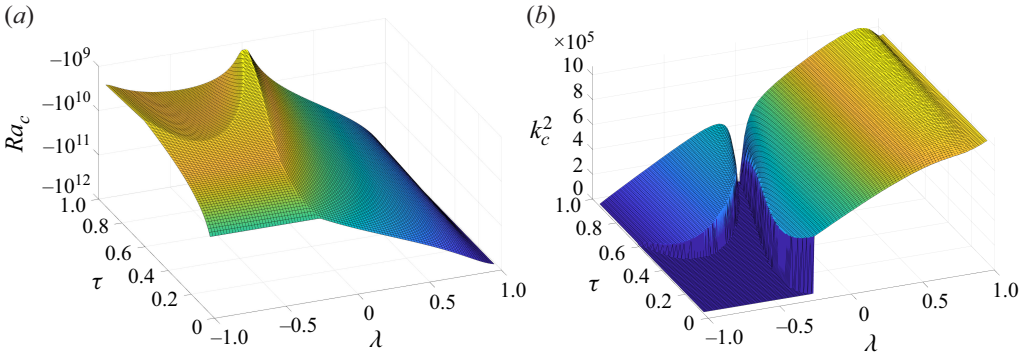


Figure 17. Surface plots of (*a*) Ra_c and (*b*) k_c^2 versus λ and τ for $\Gamma = 10^{-3}$, $Rs = -10^9$, $\sigma = 1$. The range $0.05 \leqslant \tau \leqslant 0.95$ is plotted.

surface again becomes flat after the bowl, with the steady mode preferred, before again turning downhill as the oscillatory solution is favoured.

5. Beyond the stability boundary

The foregoing analysis has been directed solely at identifying the lines of neutral stability where the preferred mode has zero growth rate. Beyond these lines the basic state is unstable, with at least one mode having positive real part. We designate the mode that has the largest real part of the growth rate as the 'gravest mode'. Note that the wavenumber corresponding to the gravest mode will normally be different from that corresponding to the (preferred) mode with the lowest value of Ra.

We have shown that M–C effects destabilise, to oscillatory modes, swathes of parameter space that are stable for the classical problem. Nonetheless, an important question is whether, in the unstable regime, the growth rate of oscillations is relatively feeble, or whether we can expect robustly growing oscillations well away from the stability boundary even for very small values of Γ when Rs is large enough.

We have provided some answers to these questions by numerically calculating growth rates, oscillation frequencies and wavenumbers for the gravest mode, over the full range of λ for small values of Γ and large values of $|Rs|$, where $|Rs| = O(\Gamma^{-n})$ with $n = 3$ and $\Gamma = 10^{-3}$ and 10^{-4}, and for the particular values $\sigma = 1$ and $\tau = 0.5$. Figure 18 shows the results for the first quadrant ($Rs > 0$); for the top row, $\Gamma = 10^{-3}$ (cf. figure 4*a–c*); for the bottom row, $\Gamma = 10^{-4}$. In this quadrant the classical instability (when $\Gamma = 0$) is oscillatory; the classical boundary is marked, and it can be seen that M–C effects greatly increase the range of instability. Figure 19 shows the results for the third quadrant ($Rs < 0$). In this case, by contrast, the classical problem has no oscillatory instabilities; the latter now become preferred over most of the parameter space owing to the M–C effect. For the top row, $\Gamma = 10^{-3}$ (cf. figure 15*a–c*); for the bottom row $\Gamma = 10^{-4}$. In both these figures, attention is restricted to cases where $Ra < Rs$, since otherwise the system would be top heavy and, hence, outside of the regime of interest for double-diffusive convection. It can be seen from both these figures that, as already discussed, there are large ranges of Ra where the basic state is unstable in the presence of M–C effects where there would be no instability in the classical case (where $Ra > Rs/\tau$ is required for direct instability and $Ra > Rs(\sigma + \tau)/(1 + \sigma)$ for oscillatory instability). Away from the stability boundary the growth rates are significant and comparable with the oscillation frequencies. For some values of λ (near -1 in the first quadrant, almost everywhere in the

https://doi.org/10.1017/jfm.2026.11340 Published online by Cambridge University Press

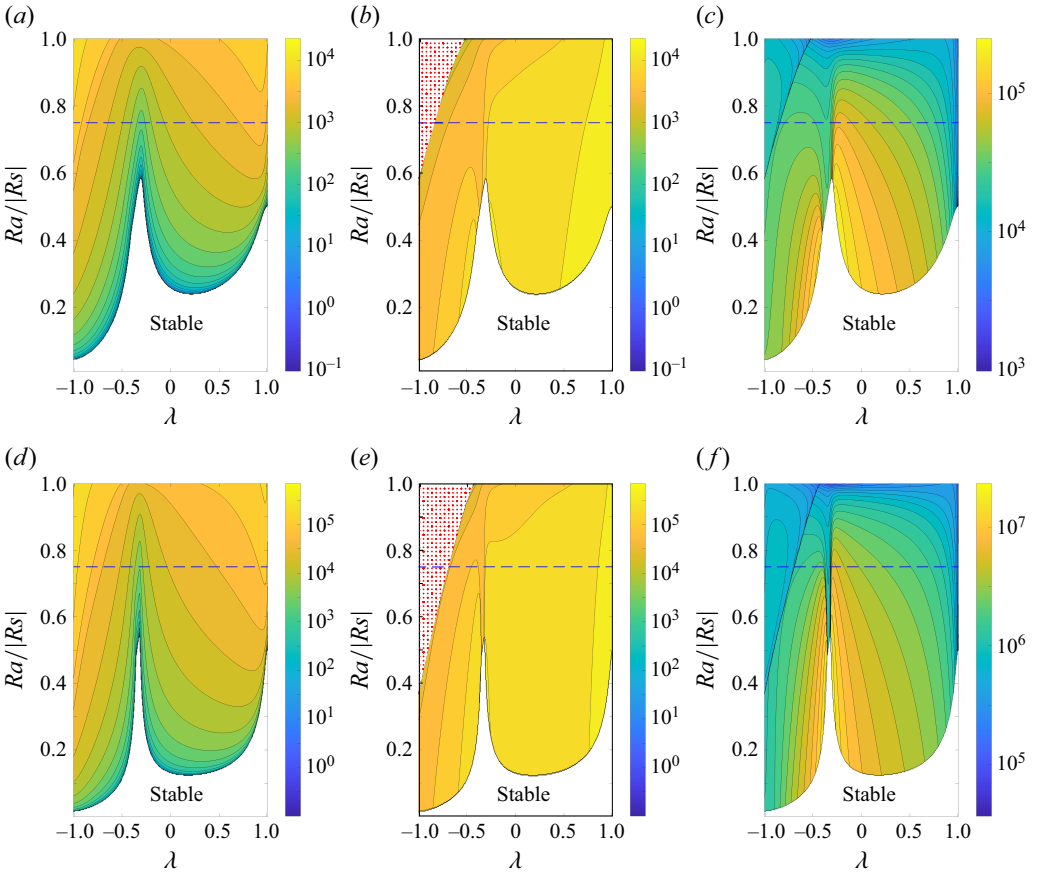


Figure 18. Contour plots as functions of λ and $Ra/|Rs|$ for (a,d) growth rate, (b,e) frequency and (c,f) k^2 for the gravest mode in the first quadrant; $\sigma = 1$, $\tau = 0.5$, for the case of $n = 3$. In the top row, $\Gamma = 10^{-3}$, $Rs = 10^9$; in the bottom row, $\Gamma = 10^{-4}$, $Rs = 10^{12}$. In plots (b) and (e), the red dotted region denotes where the gravest mode is steady. The blue dashed line shows the oscillatory stability boundary for the classical problem, given by (2.28).

third quadrant), oscillatory modes give way to steady modes as Ra is increased. We note, from a comparison of the top and bottom rows of figures 18 and 19, that reducing Γ with $Rs = O(\Gamma^{-n})$ increases the region of instability; the distinguished limit of $\Gamma \to 0$ with $Rs = O(\Gamma^{-n})$ is in marked contrast to the straightforward limit of $\Gamma \to 0$ with all other parameters fixed, which simply recovers the classical problem.

6. Conclusion and discussion

In this paper we have generalised the results presented in HPE21, in which we examined the consequences for the onset of oscillatory double-diffusive convection when the M–C effect was in operation either for the temperature or the salinity equation, but not both together. The important conclusion of that paper was that, for sufficiently large values of the salt gradient, the M–C effect has an important destabilising influence on the onset of convection, and in particular, it allows oscillations in the third quadrant where they do not appear in the classical case. This is brought about through the M–C effect introducing a new oscillatory frequency to the system, which can lead to phase relationships that are

https://doi.org/10.1017/jfm.2026.11340 Published online by Cambridge University Press

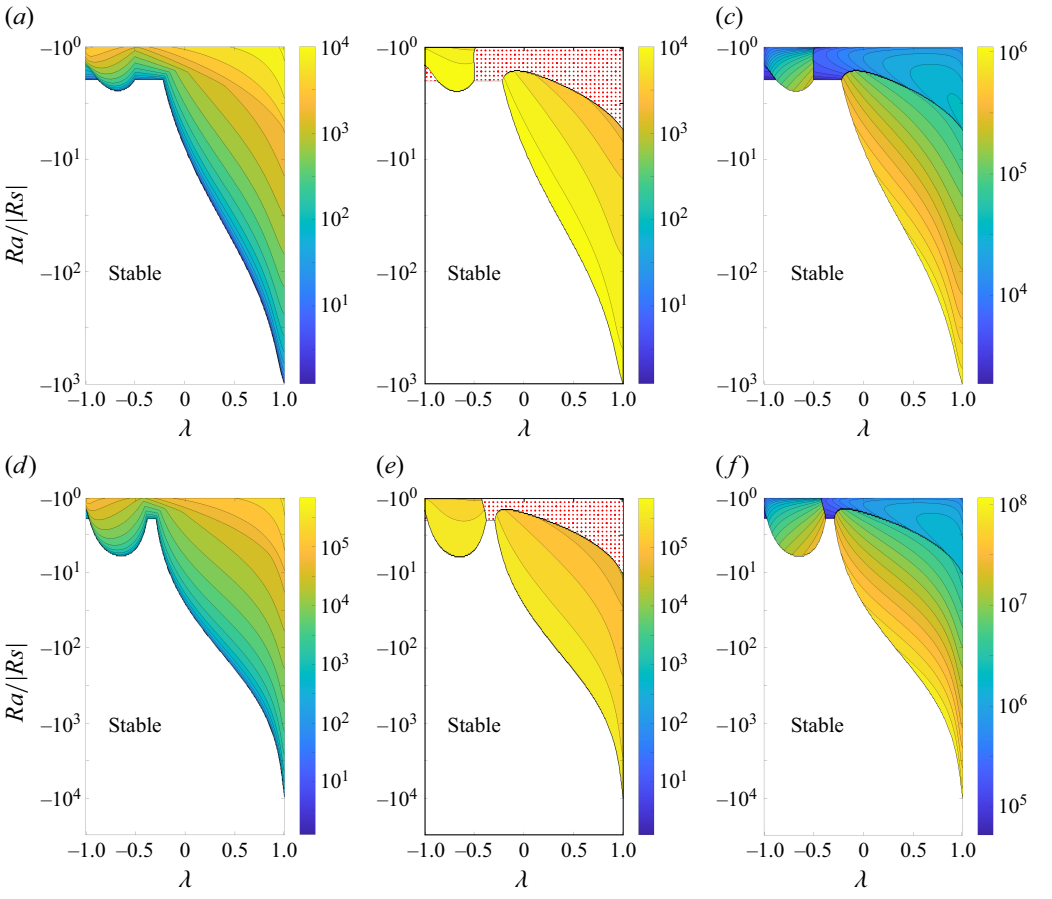


Figure 19. Contour plots as functions of λ and $Ra/|Rs|$ for (a,d) growth rate, (b,e) frequency and (c,f) k^2 for the gravest mode; $\sigma = 1$, $\tau = 0.5$, for the case of $n = 3$ in the third quadrant. In the top row, $\Gamma = 10^{-3}$, $Rs = -10^9$; in the bottom row, $\Gamma = 10^{-4}$, $Rs = -10^{12}$. In plots (b) and (e), the red dotted region denotes where the gravest mode is steady.

favourable for oscillatory instability (overstability). The scaling laws for the results in the two different cases, however, are rather different and this motivates the present study, where the M–C effect operates on both the salt and temperature fields.

In contrast to the cases investigated in HPE21, we must now consider not only the magnitudes of C_T and C_S but also their ratio; we thus introduce the quantities $\Gamma = C_T + C_S$ and $\lambda = (C_S - C_T)/(C_S + C_T)$. While we can be confident that Γ is very small, we can be less sure about the value of λ. It seems plausible on physical grounds that $\tau_S > \tau_T$; however, since $\kappa_S < \kappa$, it is hard to pin down the ratio $C_S/C_T \sim \kappa_S\tau_S/\kappa\tau_T$. One should therefore investigate the full range $-1 < \lambda < 1$.

As shown in HPE21, inclusion of the M–C effect for either temperature or salinity leads to a surprising degree of complexity compared with the classical problem, owing to the highly non-trivial dependence of the critical Rayleigh number on the wavenumber. When the M–C effect operates on both temperature and salinity, the equation determining the square of the oscillation frequency at onset, and also that determining the critical value of the Rayleigh number, becomes a cubic rather than a quadratic as in the endpoint cases of HPE21, thereby adding a further layer of complexity to the problem. Nonetheless,

https://doi.org/10.1017/jfm.2026.11340 Published online by Cambridge University Press

we have been able to carry through the analysis and determine the scalings with Γ for the values of the Rayleigh number and the critical wavenumber at onset, in many cases obtaining analytical formulae valid when n, defined by $Rs = O(\Gamma^{-n})$, is of order 2 or greater. The accuracy of these formulae has been confirmed by comparison with numerical calculations of the full system. The analysis has to be carried through separately for the first and third quadrants, as the scalings generally differ. It is assumed that (appropriately for applications) the value of Γ, representing the magnitude of the new terms, is very small. For $O(1)$ values of Rs and Ra, M–C effects are negligible. Writing $Rs = O(\Gamma^{-n})$, we find that the onset of oscillatory convection in the first quadrant is first affected by M–C effects when $n = 1$. While the critical wavenumber remains of order unity, multiple extrema of the marginal stability curve can appear. In the first quadrant (§ 3), oscillatory convection is always preferred, while multiple extrema exist for sufficiently small λ. In the third quadrant (§ 4), oscillations are not possible in this range of Rs, and M–C effects become significant only when $n = 2$.

For $n = 2$, the M–C effect appears at the same order as other effects, and the results depend on essentially all the terms in the governing equations (though for high wavenumber modes we can write $\beta^2 \approx k^2$). It is difficult to make much analytical progress in this regime and so we rely on numerical results. In the first quadrant there can be two distinct minima of Ra as a function of k^2 — one at low wavenumber and the other at high wavenumber. The two critical values of Ra are of the same order in this regime but the high wavenumber mode always wins.

In the third quadrant, on the other hand, oscillations can appear as $|Ra|$ is increased. The way in which they appear depends on σ and λ. For sufficiently small λ, oscillations appear as loops in parameter space for sufficiently small σ. These loops may appear above or below the steady branch; in the former case, oscillations become preferred as $|Rs|$ continues to increase, while in the latter case, oscillations are preferred immediately they appear. For larger values of σ, no oscillations can appear until $n \approx 3$. For larger values of λ, on the other hand, branches of oscillations will appear emanating from the steady branch via T–B bifurcations, and can subsequently become preferred.

For larger values of n, with $n \gtrsim 3$, the M–C effect generally leads to oscillatory behaviour in both quadrants, irrespective of the values of the parameters. The new phenomenon of the dip leads to completely different behaviour in the first quadrant close to the special value $\lambda = \lambda_d$, where $C_S = \tau C_T$, with a markedly reduced critical wavenumber. (In the third quadrant, steady convection becomes preferred near the dip location.) To try to understand these results – and indeed in general the underlying physical consequences of the M–C effect – we can return to the primitive equations (2.5)–(2.10). It would be ideal if the origin of the oscillatory instability could be explicated in terms of the balances between these equations, but the results for different parameter ranges show that the primary balances are not unique, and that, indeed, the determination of the stability boundary is not made at leading order but by comparing small higher-order corrections. As an example, consider the situation in the first quadrant away from the dip, for $n \geqslant 3$. Because $Ra \ll Rs$ in this regime – see the ordering (3.3) – the perturbed temperature T is much larger than the perturbed salinity S, and the leading-order equations lead simply to free oscillations in the temperature with frequency ω and wavenumber k satisfying

$$2\Gamma\lambda_2\omega^2 = k^2. \tag{6.1}$$

For general values of λ, we can find S as an oscillation at the same frequency driven by T, whose relative magnitude depends on Ra and Rs. To go further, however, and determine the size of Ra in terms of the other parameters, requires analysing the equations at higher order and a simple physical explanation seems problematic. (This approach does, however,

https://doi.org/10.1017/jfm.2026.11340 Published online by Cambridge University Press

show how the different scalings at the dip arise, since when $\lambda = \lambda_d$, there is a greatly enhanced response from S to the oscillations in T.) Similar considerations will apply in other parameter regimes.

One surprise of the present work is that the behaviour of the solutions for general λ, while not dissimilar in many ways to the results of HPE21 for $\lambda = \pm 1$, do have different asymptotic behaviours as functions of Γ. A more detailed analysis would be required to understand the transition between the asymptotic regimes as λ approaches 1 and -1, but this is not presented here; only order of magnitude estimates for the transition regions are given.

In both the first and third quadrants, when the preferred mode is oscillatory it has a small horizontal scale ($k \gg 1$) at large $|Rs|$, allowing us to approximate the total wavenumber by the horizontal wavenumber, i.e. $\beta^2 \approx k^2$. Thus, to this degree of approximation, there is a degeneracy in the vertical wavenumber m. In the numerical computations shown, we have taken $m = 1$; we have, however, also investigated the case of $m > 1$ and found that in all of the examples considered, the $m = 1$ mode is preferred. We could have simplified the equations somewhat by solving the problem in a vertically unbounded layer, although this does have the drawback that the preferred modes for the classical instability (both steady and oscillatory) have $k = 0$. Furthermore, since all the interesting instabilities induced by the M–C effect occur at large horizontal wavenumber, our main results are unchanged. The analysis of §§ 3 and 4 has revealed that new instabilities, owing their existence to the M–C effect, can occur in parameter ranges where the classical problem has no unstable modes. It is therefore of interest to explore the properties of these modes beyond the stability boundary. In § 5 we thus complement our investigations of marginal stability by calculating the gravest modes in the unstable regime, for parameter values motivated by examples studied in §§ 3 and 4. In both the first and third quadrants, these new M–C-driven modes have growth rates that are significant.

As in HPE21, we find that, in general, oscillations are preferred in both the first and third quadrants when $|Rs|$ is sufficiently large and the Prandtl number is sufficiently small. However, we have not investigated here the situations where σ scales with Γ to some power. In that case, new terms involving σ become important in the analysis and affect the asymptotic expressions. An example of the differences that can arise can be found in our parallel study of the effect of the M–C terms on rapidly rotating convection (Hughes *et al.* 2022). It turned out in that case that several different asymptotic regions exist as σ decreases, but the analysis was tractable as σ was the only relevant parameter. To do the same for the present problem would require a second extensive paper and so is left for future work.

Supplementary material. Supplementary material is available at https://doi.org/10.1017/jfm.2026.11340

Acknowledgements. D.W.H. and M.R.E.P. would like to thank the Isaac Newton Institute for Mathematical Sciences, Cambridge, for support and hospitality during the programme 'Anti-diffusive dynamics: from sub-cellular to astrophysical scales', where work on this paper was undertaken. D.W.H. would also like to thank King's College, Cambridge for the award of a Visiting Fellowship.

This paper is a memorial to D.W.H. and M.R.E.P.'s coauthor Ibrahim Eltayeb, who introduced them to the Maxwell–Cattaneo effect and inspired the present work and a number of earlier papers, but sadly passed away during its preparation for publication.

Funding. The programme at the Isaac Newton Institute was supported by EPSRC grant EP/R014604/1.

Declaration of interests. The authors report no conflict of interest.

https://doi.org/10.1017/jfm.2026.11340 Published online by Cambridge University Press

Appendix A

Although the coefficients of the full cubic equation determining the value of Ra on the stability boundary for oscillatory modes are rather complicated (see supplementary material), and much more unwieldy than those for the cubic equation determining ω^2, it is nonetheless helpful, for the $n=1$ regime, to work with the cubic for Ra, but just retaining the crucial terms. As in HPE21, we scale $Rs = \Gamma^{-1}\widetilde{Rs}$. Retaining leading-order terms in the coefficients, and, where necessary, terms of the next order, we may express an approximation to the cubic equation for Ra, symbolically, by

$$c_{35}\Gamma^5 Ra^3 + c_{23}\Gamma^3 Ra^2 + \left(c_{11}\Gamma + c_{12}\Gamma^2\right) Ra + c_{00} + c_{01}\Gamma = 0, \tag{A1}$$

where the coefficients c_{ij} do not involve Γ. At leading order, we see that the smallest and, hence, most important, root has $Ra = O(\Gamma^{-1})$; thus, again as in HPE21 we rescale $Ra = \Gamma^{-1}\widetilde{Ra}$ and write $\widetilde{Ra} = \widetilde{Ra}_0 + \Gamma\widetilde{Ra}_1$. Thus, $\widetilde{Ra}_0 = -c_{00}/c_{11}$, where

$$c_{11} = \frac{2\beta^{10}k^2\,(\sigma+1)}{\sigma^4}, \quad c_{00} = -\frac{2\widetilde{Rs}\beta^{10}k^2\,(\sigma+\tau)}{\sigma^4}, \tag{A2}$$

leading to the simple expression

$$\widetilde{Ra}_0 = \frac{(\sigma+\tau)}{(1+\sigma)}\widetilde{Rs}. \tag{A3}$$

Expression (A3) is precisely as in HPE21 (which looked at the cases of $\lambda = \pm 1$); there is no wavenumber dependence and also no dependence on λ. The wavenumber dependence enters at the next order in (A1), namely

$$c_{23}\widetilde{Ra}_0^2 + c_{11}\widetilde{Ra}_1 + c_{12}\widetilde{Ra}_0 + c_{01} = 0. \tag{A4}$$

On substituting for $\widetilde{Ra}_0$ from (A3) and for the coefficients c_{ij}, and after considerable algebra, we obtain the following expression for $\widetilde{Ra}_1$:

$$\widetilde{Ra}_1 = C_1\frac{k^2}{\beta^2} + C_2\beta^2 + C_3\frac{\beta^6}{k^2}, \tag{A5a}$$

where

$$C_1 = \frac{\sigma(1-\tau)\left[(1-\lambda)^2(\sigma+\tau) - (1+\lambda)^2\tau(1+\sigma)\right]}{(1+\sigma)^3}\widetilde{Rs}^2, \tag{A5b}$$

$$C_2 = -\frac{\left[(1-\lambda)(2+\sigma)(\sigma+\tau) - (1+\lambda)\tau(\sigma+2\tau)(1+\sigma)\right]}{(1+\sigma)^2}\widetilde{Rs}, \tag{A5c}$$

$$C_3 = \frac{(\sigma+\tau)(1+\tau)}{\sigma}. \tag{A5d}$$

Note that, for $\lambda = -1$ ($C_S = 0$), expression (A5a) reduces to expression (3.9) of HPE21; for $\lambda = 1$ ($C_T = 0$), (A5a) reduces to (4.8) of HPE21.

Stationary points ($\mathrm{d}\widetilde{Ra}_1/\mathrm{d}k^2 = 0$) are therefore given by the following polynomial, quintic in k^2:

$$2C_3k^{10} + (C_2+7C_3)k^8 + (2C_2+8C_3)k^6 + (C_1+C_2+2C_3)k^4 - 2C_3k^2 - C_3 = 0. \tag{A6}$$

The classical result $k^2 = 1/2$ is recovered by setting $C_1 = C_2 = 0$, corresponding to $\Gamma \to 0$ at fixed Rs.

https://doi.org/10.1017/jfm.2026.11340 Published online by Cambridge University Press

References

CARRASSI, M. & MORRO, A. 1972 A modified Navier–Stokes equation, and its consequences on sound dispersion. *Nuovo Cimento B Serie* **9**, 321–343.

CHRISTOV, C.I. 2009 On frame indifferent formulation of the Maxwell-Cattaneo model of finite-speed heat conduction. *Mech. Res. Commun.* **36**, 481–486.

GARAUD, P. 2018 Double-diffusive convection at low Prandtl number. *Ann. Rev. Fluid Mech.* **50**, 275–298.

HUGHES, D.W. & BRUMMELL, N.H. 2021 Double-diffusive magnetic layering. *Astrophys. J.* **922**, 195.

HUGHES, D.W. & PROCTOR, M.R.E. 1988 Magnetic fields in the solar convection zone: magnetoconvection and magnetic buoyancy. *Ann. Rev. Fluid Mech.* **20**, 187–223.

HUGHES, D.W., PROCTOR, M.R.E. & ELTAYEB, I.A. 2021 Maxwell-Cattaneo double-diffusive convection: limiting cases. *J. Fluid Mech.* **927**, A13.

HUGHES, D.W., PROCTOR, M.R.E. & ELTAYEB, I.A. 2022 Rapidly rotating Maxwell-Cattaneo convection. *Phys. Rev. Fluids* **7**, 093502.

HUPPERT, H.E. & SPARKS, R.S.J. 1984 Double-diffusive convection due to crystallization in magmas. *Ann. Rev. Earth Planet. Sci.* **12**, 11–37.

HUPPERT, H.E. & TURNER, J.S. 1981 Double-diffusive convection. *J. Fluid Mech.* **106**, 299–329.

KATO, S. 1966 Overstable convection in a medium stratified in mean molecular weight. *Publ. Astron. Soc. Japan* **18**, 374–383.

MAXWELL, J.C. 1867 On the dynamical theory of gases. *Phil. Trans. R. Soc. Lond.* **157**, 49–88.

MERRYFIELD, W.J. 1995 Hydrodynamics of semiconvection. *Astrophys. J.* **444**, 318–337.

MOHAMMADEIN, S.A. 2006 The derivation of thermal relaxation time between two-phase bubbly flow. *Heat Mass Transfer* **42**, 364–369.

NEUHAUSER, B. 1987 Thermal relaxation in super fluid helium-3. *Japan J. Appl. Phys. Suppl.* **26**, 187–188.

RADKO, T. 2013 *Double-Diffusive Convection*. Cambridge University Press.

https://doi.org/10.1017/jfm.2026.11340 Published online by Cambridge University Press